Sl. No.	IIT Ropar List of Recent Publications with Abstract Coverage: July, 2026
A	**Book Chapter(s)**
1.	Blockchain for urban welfare in the global south: A capability-driven framework for digital inclusion and sustainable impact **J Singh,** SK Chatrath, J Verma, GS Batra - Blockchain Success Stories: Real-World Case Studies in Digital Finance: Book Chapter, 2026 **Abstract:** Persistent urban poverty across India and much of the Global South remains a formidable challenge, despite rapid economic growth and ongoing efforts to digitize social welfare provision. This chapter examines how blockchain—a distributed, transparent, and immutable digital ledger—could transform urban welfare programs by fostering greater transparency, fairness, and beneficiary empowerment. Drawing on the capability approach, which emphasizes the expansion of people's substantive freedoms, the chapter highlights how blockchain-based initiatives might enhance financial inclusion and address entrenched patterns of deprivation in low-income urban communities. A critical appraisal of India's existing digital welfare tools, including Direct Benefit Transfers (DBT) and the JAM Trinity, reveals persistent barriers such as account dormancy, authentication failures, and exclusion of the most vulnerable segments. To surmount these deficits, this work proposes a three-tier architectural framework centering on inclusive governance, user-friendly smart contracts, and privacy-preserving identity systems. The analysis draws on both Indian and broader Global South case studies—such as Brazil's Bolsa Família and Kenya's digital ID—to illustrate key lessons in integrating technology with locally grounded policies. Ultimately, the chapter outlines a roadmap for policy reforms, institutional alignment, and pilot-based experimentation that could stimulate more equitable and capability-enhancing urban welfare systems.
B	**Conference Proceeding(s)**
2.	Design and simulation of stretchable crossbar array for neuromorphic computing **T Manna**…**R Sharma** - IEEE 30th Workshop on Signal and Power Integrity (SPI), 2026 **Abstract:** Flexible and stretchable systems are emerging technology in electronic system design. Flexible electronics, also known as flex circuits, are the technology that involves mounting of electronic components on elastomeric substrate. However, flexible electronics may face reliability issues under applied mechanical deformation. In this paper, a crossbar array is considered on a polydimethylsiloxane (PDMS) substrate for neuromorphic computing. To characterize the performance, the thermo-mechanical analysis is performed using finite element analysis (FEA) based model under uniaxial stretching conditions. Further, electrical analysis is performed. For this, resistance and capacitance parameters are extracted. The extracted values are subsequently utilized to perform signal integrity analysis such as S -parameter. The overall findings offer valuable insight into the operational limits and failure mechanisms of high-density crossbar array.
3.	DualCare: A blockchain framework for secure medical data sharing with dual consent **K Hemlata, S Saxena, D Barodiya, Raman, S Pal,** S Pal - IEEE International Conference on Blockchain and Cryptocurrency (ICBC), 2026 **Abstract:** The sharing of medical data plays a vital role in enhancing healthcare services and medical research, yet it also brings serious issues concerning privacy, security, and unauthorized access. The available solutions that exist in blockchain are primarily role-based access and single-level consent, which are not always enough to protect the sensitive patient information fully when

	access is permitted. To address these challenges, this paper introduces DualCare, a cross-chain consortium blockchain framework designed to share medical data through a dual consent approach across homogeneous blockchain networks. This proposed framework has a dual network model (based on Hyperledger Fabric) where hospital and patient data are kept independent within their own blockchains but remain connected through a relay service that will securely transmit consent and distribute keys between the two blockchains. Medical records are stored off-chain in MinIO and verified for integrity across both blockchains via hash values stored in the ledger. A cryptographic key management middleware module handles the keys that are used to secure hospital medical record access, including using AES-256 encrypted keys to secure hospital medical record access, RSA-2048 wrapped keys for key distribution, and a dynamic revocation model providing a time-limited access control mechanism. The complete end-to-end workflow has been implemented and experimentally validated across the dual-network topology. Experimental results show consistent transaction latency and high pipeline efficiency, demonstrating the practical feasibility of cross-chain dual consent for real-world healthcare data governance.
4.	Estimating the longitudinal impact of traditional and modern teaching methods on engineering students K Panchal, **P Kumar** - IEEE Global Engineering Education Conference (EDUCON), 2026 **Abstract:** With the increasing use of AI, engineering departments are adopting modern teaching methods more widely, yet without quantified evidence on who benefits most or what effort-outcome trade-offs to expect over a full year. Focusing on first-year engineering, we compare traditional and modern/blended teaching methods across two semesters. To obtain effect-size priors and implementation guardrails, we build a calibrated synthetic dataset of 2000 students using conditional tabular generation for baseline attributes and weekly dynamics linking preparation, engagement, assessment performance, and continuation/withdrawal. The pipeline includes automatic and human data validation; two regression views of effort–efficiency (analyzing the performance for the same number of study hours for traditional and modern approaches; analyzing the number of study hours keeping performance fixed) with standardized coefficients for interpretability and an ablation study over blend ratios to assess sustainability. Key findings indicate that blended instruction yields modest overall performance gains and meaningful Drop/Fail/Withdraw (DFW) rate reductions, with stronger effects for less-prepared students. Effort– efficiency improves in both directions: for the same study hours, predicted performance is higher; for the same target performance, fewer hours are required. We interpret the models using standardized coefficients and evaluate appropriate blends of traditional and modern teaching methods, providing effect-size priors and implementation guardrails that pave the way for subsequent real-world longitudinal field studies.
5.	Finite blocklength analysis of active and passive STARS-CR-NOMA with practical constraints S Kumar, **B Kumbhani,** K Singh, A Kaushik - IEEE International Conference on Communications (ICC), 2026 **Abstract:** This paper investigates the finite blocklength analysis of an active and passive simultaneously transmitting and reflecting surface (STARS)-assisted cognitive radio (CR) non-orthogonal multiple access (NOMA) system. By employing a transmit antenna selection (TAS) scheme, a multi-antenna secondary source operates in underlay mode to transmit information to two secondary users located in the reflection and refraction regions of the STARS using the NOMA technique. The system performance is analyzed in the finite blocklength regime while considering practical constraints such as hardware impairments (HIs) and imperfect successive interference cancellation (SIC). We derive novel closed-form expressions for the average block error rate (ABLER), system throughput, and system goodput. To provide deeper insights, asymptotic ABLER expressions are also derived under two power settings: (i) when the transmit

	power of the secondary source approaches infinity, and (ii) when the maximum interference constraint of the primary network approaches infinity. Finally, Monte Carlo simulations are performed to validate the analytical results. Numerical results confirm the superiority of NOMA over orthogonal multiple access (OMA) and compare the system performance with passive STARS. Moreover, it is shown that the diversity order depends on the number of transmit antennas and reflecting elements. The effects of blocklength, the number of transmit antennas, and HIs on system performance are also examined.
6.	FeeDeR: Fee-based bi-directional rebalancing in payment channel networks **S Mishra, S Kapoor, S Pal** - IEEE International Conference on Blockchain and Cryptocurrency (ICBC), 2026 **Abstract:** The transaction system is evolving towards online platforms but remains restricted within national borders. Cryptocurrencies break these restrictions by enabling crossborder transactions. However, scalability is still an open challenge for these cryptocurrencies. While Payment Channel Networks (PCNs) provide an efficient scaling solution, their performance is limited by channel balance depletion. This depletion lowers the number of payments when compared with a centralized payment system. In this study, we propose FeeDeR, Fee-Based Bi-Directional Rebalancing in PCNs to prevent channel depletion in both directions. This bidirectional rebalancing helps with bidirectional payments. Our algorithm outperforms existing routing algorithms, improving throughput and success rate by 1.17 times and 19.3%, respectively.
7.	Focused optical vortices with extended DOF via flat multilevel diffractive lens **A Kumari,** TM Hayward, R Menon, **V Pal** - International Conference Laser Optics (ICLO), 2026 **Abstract:** We present a new approach for generating focused optical vortices (FOVs) with an extended depth of focus (DOF) using an inverse-designed, compact, thin multilevel diffractive lens (MDL). Unlike conventional lenses, this MDL can focus an incoming OVs at a specified distance while significantly increasing the DOF. Increasing the input vortex size enhances the DOF and produces additional intensity rings that depend on the topological charge (l).
8.	Impact of image fusion of optical and microwave satellite imagery under cloudy conditions N Vyas, GK Sethi, **S Singh** - IEEE Mediterranean and Middle-East Geoscience and Remote Sensing Symposium (M2GARSS), 2026 **Abstract:** Cloud cover presents a significant challenge in optical remote sensing, often leading to incomplete or inaccurate land cover classification. This study examines a fusion-based approach that integrates Sentinel-2 optical imagery with Sentinel-1 microwave data to improve classification accuracy in cloudaffected areas. A small study area between the Panipat and Sonipat regions of Haryana, India, was selected. Principal component spectral (PCS)-based fusion was used to fuse the optical and microwave satellite imagery, followed by classification using a support vector machine (SVM). The fused classified image demonstrated higher accuracy compared to Sentinel-2 alone, with improvements confirmed through quantitative metrics and visual analysis. Cloud impact was further assessed across three selected subregions, where fusion effectively resolved misclassification issues caused by cloud obstruction. The fused outputs showed better alignment with ground truth and reference imagery, confirming the robustness of the fusion technique. This study highlights the potential of optical-microwave data fusion in improving land cover classification in cloud-prone areas. The approach provides a reliable solution for enhancing surface monitoring in operational remote sensing applications where cloud interference is frequent.
9.	Kinematic characterization of a 5-DOF exoskeleton for biomimetic shoulder movement assistance **E Singla, AK Rout** - 7th International Conference of the Robotics Society (AIR), 2026

	Abstract: This work presents the concept design and kinematic analysis of 5-degree of freedom (DoF) shoulder exoskeleton which is based on the spatial parallel mechanism with a targets to replicate natural shoulder motion. Five active prismatic actuation are being employed to align themselves with the anatomical structure expected for biomimetic motion of the shoulder complex to the closest, to enable controlled movement through SPU(Spherical-Prismatic-Universal) jointed legs. The mechanism comprises (prismatic) legged actuators with attachment end connections specifically positioned to correspond with the anatomical orientation of the major shoulder muscles. The selected actuator leg attachment positions on the torso and on the upper arm, aim to reflect the muscle line of action. Formulation of kinematics for the proposed mechanism is detailed, followed by handling the intricacies of forward kinematics through Newton-Raphson. This design is expected to provide shoulder movement patterns that closely aligns with the natural biomechanics, offering potential utility in rehabilitation and assistive field applications.
10.	MXene coupled SPR sensor for sensitivity enhancement **GP Singh, A Pandey, N Sardana** - CLEO: Science and Innovations (CLEO 2026), 2026 **Abstract:** MXenes with favourable optical properties calculated using density functional theory (DFT)(M1 x M2 y C z N z'T a) and in literature were compared as surface plasmon resonance (SPR) sensors in the Kretschmann configuration.
11.	Strata: Proactive page placement in hybrid memory systems **Upasna, VK Tavva** - 23rd ACM International Conference on Computing Frontiers (CF), 2026 **Abstract:** Hybrid memory systems that integrate high-bandwidth memory (HBM) with off-chip DRAM employ page migration mechanisms to balance performance and capacity. The state-of-the-art technique Bumblebee introduces a hotness-based page allocation mechanism in which new pages are placed in HBM only if they remain present in an HBM hot-page queue and if free HBM capacity is available; otherwise, pages are allocated in off-chip DRAM. While this approach can potentially reduce unnecessary migrations and HBM pollution, it remains conservative with respect to initial page placement. Our proposal, Strata, proactively assigns newly allocated pages to HBM, rather than deferring HBM placement until sufficient hotness history is observed. This increases the fraction of early accesses served by HBM, reducing memory access latency and improving overall IPC by 27.18% over Bumblebee.
12.	Thermal control of Q-factor in terahertz quasi-BIC metasurfaces via lanthanum m-type hexaferrites KM Rohith, S Biswas…**G Kumar** - CLEO: Science and Innovations (CLEO 2026), 2026 **Abstract:** We report a novel Lanthanum M-type hexaferrite exhibiting thermally tunable terahertz dielectric properties to actively control the Q-factor of a narrow resonance in a quasi bound-state-in-continuum metasurface. A 46.8% change in Q-factor is achieved for a temperature variation of 119 K in simulation using the experimental data of the material.
C	**Article(s)**
13.	A fractional hierarchical attention model for enhanced context-guided visual storytelling PS Yadav, DK Tyagi, **SK Vipparthi** - Information Processing & Management, 2026 **Abstract:** Visual storytelling requires generating coherent and emotionally aligned narratives from image sequences, yet existing methods often fail to preserve fine-grained visual details, temporal continuity, and affective consistency, particularly in scenario-driven settings. This work proposes a context-guided visual storytelling framework that integrates image retrieval, sequence ordering, and sentiment-aware narrative generation. The core of the framework is a Convolution Hierarchical Neural Attention Fractional Network (CHNAFN), which combines convolutional

	feature extraction with hierarchical attention and fractional calculus–based feature weighting to enhance visual representation quality. Retrieved frames are temporally organized using a Graph Convolutional Network (GCN), while emotional cues are extracted through a Multi-Layered Sentiment Extraction Module (MLSEM). The fused visual, structural, and sentiment representations are then used by the GPT-NeoX-20B language model to generate final narratives. Experiments on the VIST dataset indicate that the proposed method achieves 91.03% accuracy and a 91.33% F1-score with CHNAFN, whereas MLSEM achieves an F1-score of 90.89%.
14.	A novel missing-rib auxetic structure with central node for enhanced mechanical performance **S Kumar, CK Nirala** - Composite Structures, 2026 **Abstract:** Auxetic structures, characterized by their unconventional deformation behaviour and negative Poisson's ratio, have gained significant interest due to their improved mechanical performance. Since the inception of auxeticity, design concepts for various mechanical metamaterials have evolved rapidly. In this study, a novel two-dimensional enhanced missing-rib (EMR) auxetic structure is proposed by mirroring the classical missing-rib (CMR) auxetic structure, and incorporating an auxiliary circular node at the centre of each unit cell. The mechanical properties and deformation behaviour of the proposed EMR auxetic structure are systematically examined under quasi-static compression loading using experimental testing and finite element analysis. The effects of array size, auxiliary circular node radius and ligament thickness on deformation patterns, effective Young's modulus, effective shear modulus and negative Poisson's ratio (NPR) are examined analytically and numerically for both structures. The results demonstrate that the EMR auxetic structure exhibits improved negative Poisson's ratio, stiffness and stress distribution due to enhanced rotational deformation mechanisms. Polylactic acid is used as the base material, and specimens are fabricated using additive manufacturing technology, fused deposition modelling for testing. The experimental, theoretical and numerical results are found in good agreement. Overall, the proposed EMR auxetic structure outperforms CMR auxetic structure in all respect i.e. negative Poisson's ratio, stiffness and specific energy absorption capacity. However, the validations of the proposed model are limited to applied boundary conditions, material and laboratory-scale auxetic unit cell and array specimens. These findings provide valuable insights into the mechanical behaviour of missing-rib auxetic structures as a basis for exploring its potential in novel applications.
15.	A wiener-type criterion for fine continuity in Newton-Sobolev spaces **MA Bhat, G Kosuru** - Results in Mathematics, 2026 **Abstract:** Let (X,d,μ) be a metric measure space equipped with a doubling measure and supporting a p-Poincaré inequality, where $1 < p < \infty$. For a function $u \in N1,p(X)$, we establish a sufficient condition for fine continuity at a point in terms of the convergence of a Wiener-type integral involving its minimal p-weak upper gradient. This condition holds outside a set of zero - capacity for each $1 < q < p$, and hence yields fine continuity q-quasieverywhere.
16.	Additive free 3D printing and *in vitro* cytocompatibility analysis of jute-derived TEMPO oxidized nano-cellulose scaffolds **S Ghosh, A Mukherjee, JH Rajput, A Poundarik, B Das -** Materials Advances, 2026 **Abstract:** Cellulose, a naturally occurring biopolymer, has garnered interest in biomedical research due to its mechanical properties, biocompatibility, and tunable biodegradability. Especially, in the nanoform, cellulose is easily water-suspendable and valuable as a biopolymer. However, additive manufacturing of nanocellulose is always challenging, and primarily, 3D printing is conducted with certain additives. This limits the use of nanocellulose as a biomaterial due to its lack of repeatability, biocompatibility, and cost. In the current study, we have conducted the isolation and manufacture of TEMPO-[(2,2,6,6-tetramethylpiperidin-1-yl)oxyl]-oxidized

	cellulose nanofibers (TOCNs) from the major agricultural crop jute (*Corchorus capsularis*). The cellulose was first extracted from jute bast fibers through a series of chemical treatments, including alkaline and acid hydrolysis, followed by TEMPO-mediated oxidation to introduce carboxyl functional groups. The TOCN hydrogel was 3D-printed into scaffolds at varying concentrations, and post-printing crosslinking was performed using $CaCl_2$. The hydrogel printing was achieved without any additive or supporting polymer, but only with a combinatorial solvent system. Different physicochemical evaluations comprising Fourier transform infrared (FTIR) spectroscopy, X-ray photoelectron spectroscopy (XPS), thermogravimetric analysis (TGA), and rheological testing, validated the successful oxidation of cellulose and structural integrity of the scaffolds under simulated physiological conditions. The *in vitro* tests using mouse fibroblast (L-929) cells demonstrated enhanced cell viability, adhesion, and proliferation, with the scaffolds showing exceptional cytocompatibility. The results demonstrate the efficacy of jute-derived TOCN scaffolds as suitable biomaterials for tissue engineering applications. 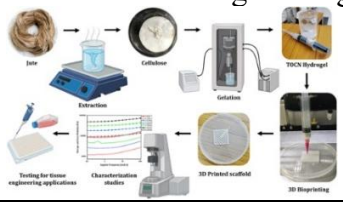
17.	AF-CANet: Augmentation-free, curriculum-guided attention UNet framework for few-shot document layout analysis **HS Kawoosa,** S Rangasrinivasan, S Setlur, **P Goyal,** V Govindaraju - Pattern Recognition Letters, 2026 **Abstract:** Pixel-precise Document Layout Analysis (DLA) is a critical step in processing historical and handwritten manuscripts that face challenges such as limited annotations and severe class imbalance. Existing few-shot methods typically rely on handcrafted data augmentation and standard semantic segmentation backbones. Moreover, the absence of pre-trained weights further restricts generalization across heterogeneous scripts. In this work, we propose AF-CANet, an augmentation-free, curriculum-guided attention-based U-Net framework for few-shot DLA. Unlike prior methods that rely heavily on handcrafted augmentation or large-scale pretraining, AF-CANet introduces an Efficient Dilated Channel Attention module to capture rich multiscale global semantic features and a cross-dataset curriculum learning strategy to enhance generalisation under limited supervision. Our model outperforms state-of-the-art methods on the DIVA-HisDB benchmark, achieving $F1$ and IoU gains of 8.96% and 8.8%, respectively, without external augmentation. Comprehensive ablation studies validate each component's contribution.
18.	Bluetooth LE audio–based energy-efficient IoT sensor system for biodiversity monitoring **R Verma, S Kumar,** L Catarinucci - IEEE Journal of Radio Frequency Identification, 2026 **Abstract:** This paper presents a Bluetooth Low Energy (BLE) audio-based sensor system for energy-efficient biodiversity monitoring, leveraging the latest Bluetooth 5.2 standard. The novelty of this work lies in the development and experimental validation of an event-driven detection pipeline integrated with the Low Complexity Communication Codec (LC3) and BLE Broadcast Isochronous Stream (BIS) mode. The proposed battery-powered sensing node enables real-time, low-power streaming of bee acoustic data. Unlike traditional continuous recording or streaming approaches that transmit all captured audio and incur high current consumption overhead, the proposed system employs LE Audio with a 48 kHz sampling rate for high-quality capture, LC3 for efficient compression, and BIS mode for connection-less broadcast transmission. By tightly coupling the real-time acoustic event detection pipeline with BLE Audio communication, the proposed system selectively streams only biologically relevant acoustic events, thereby

	minimizing redundant recordings and reducing energy usage. The transmitted acoustic data is forwarded to the cloud for remote monitoring and scalable biodiversity analytics. To the best of the authors' knowledge, this work represents one of the first practical evaluations of Bluetooth 5.2 LE Audio BIS-based real-time acoustic biodiversity monitoring in resource-constrained IoT deployments. Experimental results demonstrate about 46.8% reduction in redundant data and 28.6% reduction in energy consumption compared to continuous streaming; field tests confirm a packet delivery ratio of approximately 93% with an F1-score of 0.922, and the system is estimated to support up to 8.6 months of operation. These results highlight the suitability of the proposed BLE Audio framework for Internet of Things (IoT)-based biodiversity monitoring.
19.	Bright single-photon emission from nanowaveguide-coupled N- centers **A Redhu, RV Nair** - Physical Review Applied, 2026 **Abstract**: Realizing deterministic and bright single-photon sources with minimal two-photon probability at room temperature is essential for quantum communication, computation, and sensing. Solid-state quantum emitters, particularly nitrogen-vacancy (N-*V*) centers in diamond, are prime candidates for single-photon emission and spin addressability but suffer from limited photon extraction efficiency and higher two-photon probability. Here, we demonstrate efficient coupling of single N-*V* centers in diamond nanowaveguides to guided optical modes, enabling enhanced single-photon outcoupling with low two-photon probability. By optimizing excitation and collection geometry, we achieve a single-photon count rate of approximately 2 Mcps along with a low two-photon probability of $g(2)(0) = 0.014 \pm 0.004$. The nanowaveguide architecture overcomes alignment and bandwidth constraints of resonant cavities, providing a scalable, fabrication-compatible route for bright single-photon sources.
20.	"Calcutta weighs upon my chest, a cruel stone": The individual and the public in bengali urban poetry of the 1960s–1980s **S Das, D Ray** - Journal of Postcolonial Writing, 2026 **Abstract:** This article examines the representation of postcolonial Calcutta in 1960s–1980s Bengali poetry, emphasizing the evolving relationship between the individual and the urban public. It identifies a shared postcolonial poetics of urbanity among several Calcutta-based poets, primarily associated with the poetry magazine *Krttibās*, writing during three decades of refugee crisis, mass movements, and political disenchantment. The article shows how 1960s Bengali poetry explores frictions of urban migration through the city's intervention in poetic interiority. Producing entanglements between poetic form and political reality, the poetry of the 1970s absorbs the spirit of political collectivism and employs a realist mode to engage directly with the urban poor. In the poetry of the 1980s, this trajectory from poetic internalism to rebellious assimilation culminates in disillusionment, disorientation, and detachment. Retracing this trajectory, this article argues that postcolonial Bengali poetry captures Calcutta's history of spatial–ideological contestations through engagement and negotiation with the public.
21.	Can channel network topology govern prediction of ungauged design floods? **S Rana, AK Singh, SR Chavan** - Hydrological Sciences Journal, 2026 **Abstract:** Channel network topology (CNT) entails the spatial arrangement of internal and external nodes within the catchments and can serve as an important factor in influencing hydrological responses of catchments. Estimating hydrological responses at ungauged locations remains a major challenge in hydrology. Regional Flood Frequency Analysis (RFFA) has emerged as a reliable solution to address this challenge over recent decades. Traditionally, RFFA involves regionalization of catchments which are similar in terms of physiography, meteorology, and geography etc. A comprehensive evaluation and benchmarking of CNT-based regionalization in

	RFFA has seldom been studied in the past. This study aims to explore the utility of CNT-based regionalization in estimation of design floods in ungauged catchments of Peninsular India and Appalachian catchments of USA, through conventional index flood and recent transformation-based RFFA approaches. Results indicate that the CNT-based regions are indeed homogeneous and are found to be effective in prediction of ungauged design floods.
22.	Coefficients and integral mean estimates for harmonic mappings via quasi-subordination **J Parashar, SK Anbareeswaran** - Canadian Mathematical Bulletin, 2026 **Abstract:** In this paper, we study normalized univalent harmonic mappings associated with quasisubordination. For the class S 0 q (S), we establish the harmonic analogue of the Bieberbach conjecture together with the corresponding sharp growth estimate. Under suitable additional assumptions on the quasi-subordination data, we obtain integral mean estimates for this class. We also derive analogous results for several significant subclasses of S 0 , including the class of mappings with m-fold symmetric analytic and co-analytic parts, as well as the class of mappings admitting minimal surface lifts. By leveraging the flexibility of quasi-subordination, these findings extend and unify several earlier results in the study of univalent harmonic mappings.
23.	Comprehensive TCAD-based geometry study on self-aligned coplanar top gate a-IGZO TFTs **N Choudhary,** A Daus, A Lahgere, **G Gupta, P Duhan** - APL Electronic Devices, 2026 **Abstract:** Amorphous oxide semiconductor-based thin-film transistors (TFTs) are preferred for large-area, high-resolution displays and memory applications owing to their superior electrical properties. However, the geometry of TFTs plays a vital role in determining the device characteristics. In this study, we present a comprehensive study of the impact of planar and stepped self-aligned coplanar geometry designs on the digital circuit performance. We adopted a mixed-mode simulation approach using technology computer-aided design simulations to design logic gates and a three-stage ring oscillator (RO) circuit. The results indicate that the stepped geometry shows better switching performance with a higher gain of 15.45 V/V but exhibits a lower oscillation frequency ($f_{osc} \sim$ 6.25 MHz), which is nearly half of the planar geometry ($f_{osc} \sim$ 14.5 MHz). Here, we present a simplified methodology that relates geometry electrostatics, and parasitic components to the RO circuit delay response. The calculated propagation delay of stepped geometry is 2.31 times that of planar geometry, which results in higher f_{osc} in planar geometry. A lower depletion capacitance (resulting from reduced dopant diffusion) and comparable accumulation capacitance (slope extension profile) indicate better gate control in stepped geometry. However, the threshold voltage is the primary factor that mainly contributes to the effective resistance of the geometry and affects f_{osc} and the switching behavior.
24.	Coupled hydrological–hydrodynamic modelling of GLOFs triggered by extreme precipitation in the western Himalayas **D Gaikwad, D Iawphniaw, VS Jadoun, RK Tiwari,** B Pradhan - Journal of Hydrology: Regional Studies **Abstract:** Study region Western Himalayas (Himachal Pradesh). Study focus Glacial Lake Outburst Floods (GLOFs) are increasingly recognized as a major cryosphere-related hazard in the western Himalayas, where accelerated glacier retreat, elevation-dependent warming, and intensifying extreme hydro-meteorological events collectively amplify downstream flood risk to settlements and infrastructure. Most existing GLOF hazard assessments treat lake outburst processes and extreme rainfall-induced flooding independently, potentially underestimating worst-case flood magnitudes and inundation extents. To address this critical gap, the present study integrates Extreme Rainfall Events (EREs), including Probable Maximum Precipitation (PMP), into a coupled hydrological–hydrodynamic modelling framework to assess compound GLOF–flood hazards in glacier-fed Himalayan basins. New hydrologic insights Two high-risk glacial

	lakes in the Beas and Sutlej river basins were analysed using coupled HEC-HMS and HEC-RAS models under multi-return-period flood scenarios (2–100 years) and the Probable Maximum Flood (PMF). PMF discharges peaked at 17,086 m^3 /s at Pandoh Dam and 23,478 m^3 /s at Bhakra Dam, with model validation showing strong performance (Nash–Sutcliffe Efficiency > 0.65 and > 0.75). Incorporating PMP-based discharges into GLOF simulations enabled worst-case combined GLOF-PMF modelling, yielding peak flows of 17, 356 m^3 /s (Beas) and 24,723 m^3 /s (Sutlej). Inundation mapping revealed major risks to hydropower projects, religious sites, and over 680 structures. Given the projected intensification of extreme precipitation under climate change, this integrated approach is readily transferable to other glacierized basins across the Himalayas. 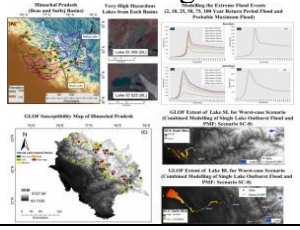
25.	Deep random vector functional link network for anomaly detection **M Ganaie,** NS Uddin, M Wasid, J Imran, R Ali - Expert Systems with Applications, 2026 **Abstract:** The Random Vector Functional Link (RVFL) neural network has been successfully applied to classification and regression problems. RVFL and its deep versions have received significant attention as they optimize the weights in the output layer via a non-iterative approach. Recent works, such as shallow and ensemble deep neural networks, have been proposed for one-class classification. The shallow OC-RVFL employs a single hidden layer, while the ensemble deep neural network (OC-edRVFL) exploits the deep architecture. However, OC-edRVFL optimizes the output layer weights via repeated use of the original features, which may lead to redundant information. In this paper, a deep Random Vector Functional Link neural network is formulated for one-class classification/anomaly detection (dRVFLOC). The proposed dRVFLOC exploits the deep architecture while avoiding redundant reuse of the original features. The proposed architecture fuses linear and non-linear randomized features generated via hierarchical feature representation. The hidden layer parameters are randomly initialized within a suitable range and kept fixed. These layers are stacked to improve feature representation, and the weights of the output layer are optimized via a closed-form solution. We have evaluated the baseline and proposed dRVFLOC on multiple benchmark datasets across various domains. Experimental results show that dRVFLOC achieves the better or competitive performance on the majority of benchmarks, including non-biomedical datasets (Glass Building, Ionosphere, Iris, Flag), and biomedical domain—such as diagnosis of Alzheimer's disease and breast cancer classification—while retaining a closed-form output solution and competitive training times.
26.	Detecting the undetectable: An enhanced GAN-BERT framework with ensemble learning, statistical features, and watermarking for robust AI-generated text detection **SS Zample, A Kaushik** - Knowledge and Information Systems, 2026 **Abstract:** The proliferation of advanced Large Language Models (LLMs) such as GPT-4o, Claude-3.5, Llama-3.1, and Gemini-1.5 has rendered AI-generated text increasingly indistinguishable from human-authored content, posing profound risks to academic integrity, journalistic authenticity, and information ecosystems. This paper introduces Ensemble-GAN-BERT, an advanced detection framework that synergistically combines a Generative Adversarial Network (GAN) augmented BERT architecture with a multi-model ensemble (BERT, RoBERTa, DeBERTa-v3), hand-engineered statistical linguistic features (e.g., entropy, burstiness, POS distributions), and optional watermark probing to achieve unprecedented robustness against adversarial attacks like paraphrasing. To address resource constraints, we propose a distilled

	variant achieving comparable performance on edge devices. Extensive evaluations on seven diverse benchmarks RAID, M4, HC3, TuringBench, and others demonstrate our framework attains state-of-the-art performance with an average accuracy of 95.8%, 0.96 F1-score, and 0.97 ROC-AUC. Notably, under strong paraphrasing attacks (e.g., T5-XXL, DIPPER), our method sustains 88–92% accuracy, outperforming baselines like DetectGPT (dropping to 4–70%) and GhostBuster (70–80%) by 15–25% margins. We further evaluate industrial tools (Turnitin, Grammarly) and complex attacks (cross-modal, long-text redundancy), revealing practical generalization gaps addressed via targeted enhancements.
27.	Effects of rotational ground motions on floor acceleration demands in reinforced-concrete buildings A Jain, **M Surana** - Journal of Earthquake Engineering, 2026 **Abstract:** The influence of rotational ground motions on floor acceleration responses in eight regular reinforced-concrete moment-resisting frame buildings are examined. A total of 4,800 bi-directional and tri-directional time-history analyses were conducted across five seismic demand levels using a suite of far-field earthquake records and simulated rotational ground motions. The results indicate that rotational ground motions can amplify peak floor acceleration and total acceleration at floor edges up to 45% and 121%, respectively, particularly in short-period inelastic buildings. Simplified recommendations are proposed and validated to account for the effects of rotational ground-motion into seismic design of acceleration-sensitive secondary systems in reinforced-concrete buildings located at far-fault sites.
28.	Electronic engineering of donor–acceptor covalent organic frameworks via fluorine substitution for efficient solar hydrogen production **H Gupta,** A Chakraborty, **D Dange,** RS Pillai, **TJ Dhilip Kumar,** P Pachfule, **CM Nagaraja** - Small, 2026 **Abstract:** Covalent organic frameworks (COFs) are gaining prominence in photocatalysis due to their adjustable topologies, expanded π-conjugation, large surface areas, and superior chemical stability. Their modular architecture enables accurate control over electronic properties by rational design using appropriate building parts. Herein, we design and synthesize four pyrene-based COFs by systematically varying the number of fluorine substituents in the framework, using organic linkers containing no fluorine (Py-3Ph), mono-fluoro (Py-1Fl), difluoro (Py-2Fl), and tetrafluoro (Py-4Fl) groups. All four COFs exhibit high crystallinity and permanent porosity with distinct optoelectronic properties. These changes in the number of fluorine substituents in the structural unit of COFs have led to pronounced differences in their light absorption, charge transport, and redox potentials, ultimately resulting in different photocatalytic hydrogen evolution activities. Specifically, Py-2Fl COF showed the best H_2 evolution rate (HER) of 7150 μmol g^{-1} h^{-1} over visible light in the presence of a cocatalyst (1 wt.% Pt). Notably, the COF exhibits appreciable HER activity (614 μmol g^{-1} h^{-1}) even without a platinum co-catalyst and retains its structural stability and catalytic activity even after multiple reuse cycles. This work offers important insights into rational engineering of the structure-property-performance of COFs for improved photocatalytic HER by tuning the number of fluorine substituents in the framework.
29.	Electronic waste-to-catalyst upcycling: Selective lignin C–O bond hydrogenolysis and RCF over a Cu–iron oxide/P-doped carbon catalyst **A Chauhan, S Bhandari, R Ghalta,** R Bal, **R Srivastava** - ACS ES&T Engineering, 2026 **Abstract:** The development of sustainable catalysts from secondary waste resources provides an attractive strategy for addressing both electronic-waste management and biomass valorization challenges. In this work, a multifunctional heterogeneous catalyst (ML@ATP_1/CP_2-60) was constructed by integrating copper recovered from a discarded motherboard, toner powder-derived

	iron oxide, and phosphorus-doped carbon derived from chitosan as a heteroatom-engineered support. Comprehensive structural and surface characterization using XRD, Raman spectroscopy, XPS, HR-TEM, EPR, and temperature-programmed desorption analyses confirmed the formation of mixed-valence Cu species anchored on a defect-rich spinel iron oxide framework with interfacial acidic sites associated with iron oxide and P–O functionalities. The catalyst exhibited excellent activity and selectivity for the hydrogenolysis of benzyl phenyl ether, achieving complete conversion with exclusive formation of phenol and toluene via selective cleavage of the benzylic C(sp^3)–O bond without aromatic ring hydrogenation. Mechanistic investigations, including selective poisoning experiments, revealed a cooperative dual-site pathway involving Cu-mediated hydrogen activation and adjacent acidic centers responsible for ether bond polarization. Importantly, the catalyst demonstrated effective performance in the reductive catalytic fractionation of wheat straw, affording aromatic monomers with molecular-weight distributions comparable to those obtained using conventional 5 wt % Ru/C while suppressing deep aromatic hydrogenation. CHEM21 green metrics analysis confirms the near-ideal intrinsic reaction efficiency of the protocol (AE ≈ 100%, RME = 97.6%), with solvent usage identified as the primary contributor to process-level mass intensity. These results highlight a strategy for transforming multiple waste streams into efficient catalytic platforms for selective lignin valorization. 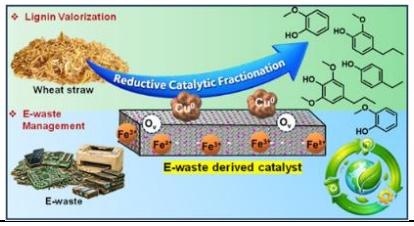
30.	Engineering an electrode–electrolyte interphase for ultrastable aqueous aluminium–air battery **K Garg, S Kaur, K Kumar, SK Meena, TC Nagaiah** - Angewandte Chemie, 2026 **Abstract:** Aluminium-air battery (Al-air battery) stands at forefront of next-generation energy storage technologies; however, their practical implementation is critically hindered by uncontrolled hydrogen evolution reaction (HER) and rapid anode degradation in alkaline environment. Herein, we explored multifunctional boric acid (BA) as an additive that orchestrates electrolyte-electrode interactions by simultaneously functioning as pH buffer, hydrogen-bond regulator and Al^{3+} solvation shell modulator. This synergistic effect driven the formation of boron-rich, self-protective aluminium oxide layer, as elucidated through scanning electrochemical microscopy (SECM) investigations, in-situ electrochemical Raman spectroscopy and x-ray photoelectron spectroscopy (XPS) analysis. Thus, introduction of BA inhibited the Al corrosion rate by 82.7% and enabled Al-air battery stability upto 302 h over 906 cycles. HER suppression was substantiated by molecular dynamic simulations and SECM-derived kinetic analysis, where heterogeneous electron transfer rate constant decreased from 9.94 * 10^{-4} cm s^{-1} in 1 M KOH to 8.80 * 10^{-4} cm s^{-1} upon addition of boric acid. The optimized Al-air battery successfully powered a panel of 38 blue LEDs for 28.5 h, underscoring its practical applicability. 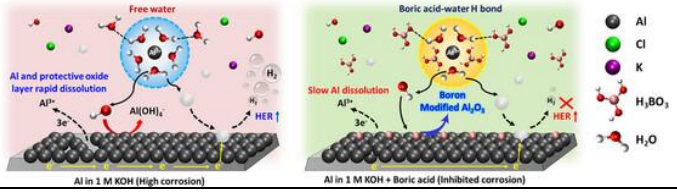
31.	Engineering short-range correlation in bi-disperse self-assembled photonic structures **K Singh, M Aleem, RV Nair** - Journal of Applied Physics, 2026

	Abstract: Short-range correlations in disordered photonic structures composed of sub-micrometer scatterers can give rise to correlation-driven photonic gaps. However, methods to systematically tune such structural correlations remain limited. Here, we investigate that the scatterer size ratio (β) in self-assembled bi-disperse photonic structures provides a pathway to engineer short-range correlations and hence the photonic gaps. Correlation-induced reflectivity peaks, accompanied by simultaneous dips in both the transport (l_t) and scattering (l_s) mean free paths, emerge over the range of $0.77 < \beta < 0.83$. Further reduction in β value suppresses short-range correlations and consequently eliminates the photonic gap. Pair correlation and structure factor analyses reveal that the observed transition from well-resolved to vanishing gaps is driven by the breakdown of short-range correlations. Experimentally extracted l_t and l_s further show that enhanced backscattering is associated with short-range correlations. Moreover, tuning the β value not only shifts the gap wavelength but also modulates its strength, as supported by finite-difference time-domain simulations. Together, these results advance disorder-enabled design strategies for photonic materials, enabling precise control of scattering and bandgap characteristics.
32.	Environmental, social and governance (ESG) dimensions and bank performance: A systematic literature review **S Chakraborty, S Bardhan,** K Dalal - Business Strategy and the Environment, 2026 **Abstract:** This paper conducts a systematic literature review (SLR) on ESG and bank performance relationship by identifying, evaluating and synthesising existing research following the guidelines of Preferred Reporting Items for Systematic Reviews and Meta-Analyses (PRISMA). The paper analyses 36 selected articles based on two search engines—Scopus and Web of Science—appropriate keywords and inclusion as well as exclusion criteria, respectively. Analysis of the reviewed articles identifies six themes based on the evidence of varying associations between ESG and bank performance, the role of corporate governance in enhancing bank performance, the role of audit quality as a moderating variable between ESG and bank performance, the fintech and ESG performance of banks, the role of bank competition in enhancing the ESG performance of banks and evidence of the application of alternative panel regression techniques. Findings reveal that ESG generally enhances long-term stability and risk management practices of banks by reducing systemic risk and, thereby, helps to build the reputation of the banking system. Our analysis further reveals that whereas social and governance pillars of ESG provide mixed evidence, environmental initiatives consistently yield the strongest positive financial and reputational outcomes. In particular, environmental and governance issues create lasting impacts on banks' businesses and mitigate adverse consequences on society and the environment. Findings also reveal that integrating a bank's ESG performance into bank competition and fintech would enhance business ease and create significant societal value. The study further shows that audit quality acts as a governance mechanism in the relationship between ESG and bank performance in emerging markets and becomes instrumental in mitigating information asymmetry and enhancing trust among shareholders.
33.	Existence and uniqueness of solution for coagulation and collisional breakage equation in a new singular space D Ghosh, DC Chang, JC Yao, **J Kumar** - Advances in Applied Mathematics, 2026 **Abstract:** In this research note, we establish the existence of a solution to the coagulation and collisional breakage equations. To this end, we introduce a new function space denoted by Ωλ,r(T)[jls-end-space/], which consists of all continuous functions f bounded by the following norm: (formula presented) This function space facilitates the analysis of singular kernels. Furthermore, we prove the volume conservation property and establish the uniqueness of the solution. The above result is verified by a numerical example.

34.	[Expanding the horizons of magnetic hyperthermia from precision medicine to artificial intelligence and smart technologies] Yashwant, **S Singh,** BK Sahoo, M Dan - Journal of Materials Chemistry C, 2026 **Abstract:** Magnetic hyperthermia (MH) has become a versatile and effective technique that leverages magnetic nanomaterial's distinctive ability to convert electromagnetic energy into localized heat when subjected to an alternating magnetic field. MH originated from preliminary research on heat-induced tumor ablation and has evolved into an advanced framework of growing significance in both biological and technological domains. This review provides a comprehensive overview of the principles, mechanisms, and recent advances in magnetic hyperthermia, emphasizing the design and functional properties of diverse magnetic nanomaterials, including iron oxides, ferrites, and metallic nanoparticles. The mechanisms of heat generation *via* Néel and Brownian relaxation, along with hysteresis losses, are comprehensively analyzed, highlighting the influence of critical parameters, including specific absorption rate (SAR), alternating magnetic field (AMF) configurations, particle morphology, and surface engineering, on thermal efficiency. The biomedical applications of MH are thoroughly discussed, emphasizing its function in oncology treatment, tumor microenvironment-responsive systems, and synergistic integration with immunotherapy, photothermal, and sonodynamic approaches. Additional emphasis is placed on heat-triggered drug and gene delivery, anti-infective treatments, image-guided interventions, and thermal stimulation for tissue engineering and regenerative medicine. Beyond healthcare, MH demonstrates significant potential in non-biomedical sectors, particularly in advancing temperature regulation for semiconductor devices, microfluidic systems, and environmental remediation. The review continues by addressing forthcoming frontiers, such as multimodal nanohybrids for theranostics, AI-driven personalized hyperthermia therapies, smart wearable or implantable hyperthermia devices, and integration of quantum and spintronic principles in magnetothermal science. Together, these advancements are shaping the next generation of hyperthermia technologies that are sustainable, precise, and therapeutically relevant. 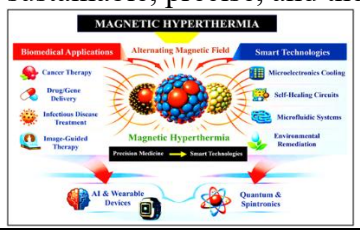
35.	[Experimental and numerical investigation on directional rigidity of face modified lattice structures] Avinash, M Mursaleen, **N Kumar** - Mechanics of Solids, 2026 **Abstract:** Due to their exceptional mechanical strength, low density, high porosity, favorable specific stiffness and remarkable energy-absorbing performance, lattice structures have become the focus of growing research interest. Their distinctive characteristics enable applications across biomedical, acoustic, defense, automotive and aerospace fields. This study employs both computational modeling and experimental testing to explore the directional stiffness of four face-modified lattice designs. Specimens were produced via Fused Deposition Modeling (FDM). The findings offer important insights into their mechanical performance and prospective engineering applications. The highest compressive strength 8.05 MPa was observed by the Vertical Opposite Triangles Face Cubic (VOTFC) structure, which was around 66.7% stronger than the Cubic Structure (CS), almost 149.2% stronger than the Triangle Face Cubic (TFC) and nearly 17.4% stronger than the Vertical Strut Face-Centered Cubic (VSFCC). With an energy absorption capacity of 1.94 MJ/m^3, the VSFCC, on the other hand, demonstrated the highest capacity, outperforming CS by about 2325, TFC by 3133, and VOTFC by 334%. The Vertical Strut Face-Centered Cubic (VSFCC) structure exhibited the maximum specific energy of 148.09 MJ/kg out

	of all the designs. The Digital Image Correlation (DIC) approach was performed to observe the lattice structures' deformation patterns.
36.	Experimental, thermodynamic, and economic analysis of a novel small-scale thermoelectric power generation system **R Goswami, R Das, S Ganguly** - Energy Sources, Part A: Recovery, Utilization, and Environmental Effects, 2026 Thermoelectric generators coupled with solar ponds offer a promising pathway for converting stored solar thermal energy into electricity. However, conventional thermosyphon-assisted thermoelectric power generation systems are often limited by significant thermal resistance during heat transfer and a low heat source temperature, which reduces the effective hot-side temperature of thermoelectric generators, consequently lowering the temperature gradient and electrical output. To address this limitation, the present study proposes a thermoelectric array-based power generation system designed to minimize thermal resistance and enhance heat transfer from the heat source to hot-side of the thermoelectric. The proposed system is experimentally integrated with a solar pond operating under real ambient conditions, and its performance is further evaluated under controlled temperatures simulating low-grade industrial waste heat sources for clean energy and decarbonization, followed by thermodynamic performance. Finally, the feasibility of the system via economic and environmental assessment is investigated. The results demonstrated that a maximum output power of 7.238 W was achieved with an open-circuit voltage and a short-circuit current of 93.67 V and 0.305 A, respectively, at a source temperature of 80 °C. The conversion and exergy efficiency of the TEG are found to be 4.78% and 34.42%, respectively. The thermal resistance barrier is reduced to 0.012 °C/W, leading to a performance improvement of 1.7–3 times higher than that of previously reported thermosyphon-based systems. The system has achieved an electricity generation cost of 8.96 INR/kWh and reduced CO_2 emissions by 85.14 kg/year, demonstrating its potential for sustainable low-grade thermal energy recovery and industrial decarbonization.
37.	Extended cut groups À García-Blàzquez, **G Kaur,** S Maheshwary - Journal of Group Theory, 2026 **Abstract:** A finite group G is said to be a cut group if all central units in the integral group ring $\mathbb{Z}G$ are trivial. In this article, we extend the notion of cut groups, by introducing extended cut groups. We study the properties of extended cut groups analogous to those known for cut groups and also characterize some substantial classes of groups having the property of being extended cut. A complete classification of extended cut metacyclic groups is presented.
38.	Facet-directed growth of spiky gold datura-shaped nanoparticles as SERS platforms enabling the detection of psychotropic and explosive molecules K Bhardwaj, **K Kumar, L Dhanda, PP Fuaadh Saneen, SK Meena,** A Jaiswal - ACS Applied Nano Materials, 2026 **Abstract:** Rationally engineered anisotropic plasmonic nanostructures offer exciting opportunities for molecular-level sensing. Here, we report the surfactant-guided synthesis and application of gold nanodaturas (Au-NDs) — a class of spike-covered, seedpod-like nanostructures—for flexible, ultrasensitive surface-enhanced Raman scattering (SERS) platforms. The anisotropic growth of Au-NDs was achieved via faceted overgrowth on pentatwinned seeds in a binary surfactant environment, cetyltrimethylammonium bromide (CTAB) and benzyldimethylhexadecylammonium chloride (BDAC), enabling precise control over particle morphology and size. Molecular dynamics simulations provided mechanistic insight, revealing that surfactant micelle density and counterion effects modulate facet-selective deposition, with dense CTAB/BDAC coverage on Au (110) facets suppressing growth and promoting edge-directed

	elongation. This atomistic understanding explains the emergence of the spiky nanodatura morphology. Exploiting their intense plasmonic hotspots arising from the sharp tips, Au-NDs were immobilized on both Whatman paper and thermally wrinkled shrink films to fabricate flexible SERS substrates. The shrink-induced nanoscale clustering significantly enhanced SERS activity, enabling detection of 1,4-benzenedithiol down to 10^{-16} M. Furthermore, real-world analytes, including Δ^9-tetrahydrocannabinol (THC) and picric acid (TNP), were detected without labels or surface modification, with high spectral reproducibility. Together, our integrated experimental–computational approach offers a robust, scalable route to tunable plasmonic architectures for field-deployable chemical sensing. These nanodatura-enabled SERS platforms hold promise for forensic diagnostics, drug screening, and explosive residue detection in point-of-care and security applications. 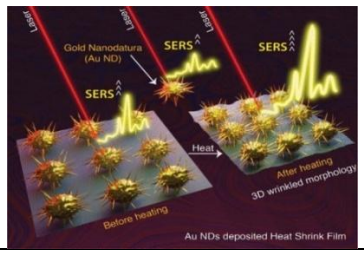
39.	FedTrust-UNLEARN: Trust-aware federated learning with auditable unlearning for privacy-preserving consumer IoMT EEG intelligence RK Rai…**A Sharma,** THH Aldhyani, S Basheer, M Kumar - IEEE Transactions on Consumer Electronics, 2026 **Abstract:** The growing adoption of EEG-enabled consumer Internet of Medical Things (IoMT) devices and wearable neuro-monitoring systems in healthcare and home-centric environments has raised critical concerns regarding data privacy, trust, and regulatory compliance. Although centralised deep learning approaches achieve strong performance in EEG-based emotion and cognitive state recognition, their reliance on centralised data aggregation limits scalability and applicability in privacy-sensitive consumer healthcare settings. Furthermore, existing federated learning approaches often inadequately address trust heterogeneity, non-IID neurophysiological variability, unreliable client participation, and the emerging requirement of federated unlearning in distributed IoMT environments. This paper proposes FedTrust-UNLEARN, a trust-aware federated learning framework with auditable unlearning for privacy-preserving EEG intelligence across heterogeneous consumer IoMT networks. The proposed framework integrates adaptive spectral representation learning, dynamic trust-aware aggregation, and an auditable federated unlearning mechanism that enables selective attenuation of client influence without requiring complete retraining. Extensive experiments on the SEED, SEED-IV, and DREAMER datasets under subject-dependent and subject-independent settings demonstrate competitive performance relative to centralised learning while improving robustness against unreliable clients, privacy preservation, and practical unlearning behaviour. The results demonstrate stable collaborative optimisation, bounded post-unlearning degradation, and communication-efficient deployment, highlighting the practicality of trustworthy, regulation-aware federated EEG intelligence for real-world consumer IoMT healthcare applications.
40.	Four-phonon-limited lattice thermal transport in a two-dimensional MBene **A Sharma, V Shukla** - The Journal of Physical Chemistry C, 2026 **Abstract:** Accurate prediction of lattice thermal transport in low-dimensional materials requires a rigorous treatment of anharmonic phonon scattering beyond the conventional three-phonon framework. Here, we present a fully *ab initio* investigation of four-phonon-limited lattice thermal transport in monolayer TiB_2, a representative two-dimensional MBene. Harmonic and higher-order interatomic force constants obtained from density functional theory are combined with an

	iterative solution of the phonon Boltzmann transport equation to explicitly resolve the competing roles of three-phonon and four-phonon scattering over a broad temperature range. Analysis of the weighted phonon phase space and frequency-resolved scattering rates reveals a rapid activation of four-phonon channels with increasing temperature. While three-phonon processes dominate thermal resistance at low and intermediate temperatures and yield an approximate inverse-temperature scaling, $\kappa \sim T^{-1}$, explicit inclusion of four-phonon scattering reduces the room-temperature lattice thermal conductivity by approximately 27% and induces a systematic breakdown of conventional T^{-1} behavior at elevated temperatures. Despite this strong renormalization, the pronounced in-plane thermal conductivity anisotropy remains robust, reflecting intrinsic anisotropy in phonon dispersions and transport velocities. The predicted room-temperature lattice thermal conductivity is nearly 2 orders of magnitude lower than representative MXenes, more than an order of magnitude lower than typical transition-metal dichalcogenides, and orders of magnitude lower than graphene, underscoring the exceptionally suppressed heat transport in two-dimensional MBenes. These results establish quartic anharmonicity as essential for quantitatively reliable thermal transport predictions and provide a direct microscopic link between multiphonon phase-space growth, enhanced four-phonon scattering, and temperature-dependent transport scaling in low-dimensional metallic lattices. 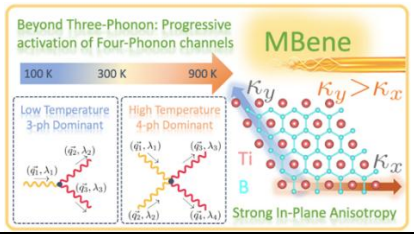
41.	Full-field mapping of spatially varying polarization entanglement generated from spontaneous parametric down-conversion C Li, **G Kulkarni**…R Boyd - Physical Review Applied, 2026 **Abstract:** Two-photon states generated from spontaneous parametric down-conversion (SPDC) can display entanglement in all degrees of freedom (DoFs) of light, including spatial, temporal, and polarization. The coupling between different DoFs of a two-photon state has been shown to display rich structures that enable novel and robust information processing schemes. While the existing literature has studied these couplings by postselecting the SPDC field, a comprehensive understanding of the inherent spatial-polarization coupling produced in the SPDC process is still lacking. This work produces a full spatial map of the polarization entanglement generated across the entire SPDC field, which contains an entire class of near-maximally polarization-entangled states with an average concurrence of 0.8303±0.0004. The spatial-polarization coupling manifests as radially or linearly varying polarization-entangled states, whose wavefunctions are dependent on the transverse momenta of the down-converted photons and the pump beam, respectively. Our study lays important groundwork for further exploiting the coupling between entanglement in different DoFs for future quantum technologies.
42.	Ga2O3 microrods-functionalized In2O3 nanostructures for a low-temperature hydrogen gas sensor S Kumar, MR Florek, **P Rani, M Kumar,** S Sahu, M Kwoka-Czornik, M Kumar - International Journal of Hydrogen Energy, 2026 **Abstract:** Due to their low cost and easy manufacture, metal oxide semiconductor (MOS) sensors like indium oxide (In_2O_3) can detect H_2, but their sensitivity and selectivity are generally restricted. Noble metal nanoparticles (NPs) can enhance sensing, but their high cost prevents widespread use. Gallium oxide (Ga_2O_3), on the other hand, is abundant and cost-effective. This study created a high-performance H_2 sensor using In_2O_3 nanostructures produced via reactive gas vacuum evaporation (RGVO) and functionalized with Ga_2O_3 microrods. Optimal operating temperature for

	the Ga_2O_3/In_2O_3 device is 50 °C. The device responded ~51% to 20 ppm H_2, twice compared to the bare In_2O_3 sensor. The sensor strongly preferred H_2 over other gases. The sensor has good response, recovery, durability, and repeatability. Enhanced sensing capability at 50 °C is achieved by the combination of In_2O_3 nanostructures and high surface area Ga_2O_3 microrods. This study proposed a low-cost, energy-efficient H_2 sensing technology, making significant advancements. 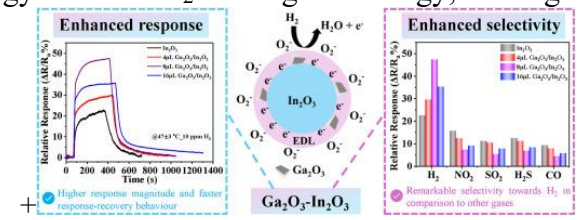
43.	Generating room temperature defect bound excitons in vanadium doped WS_2 monolayers B Luhar, **R Dhankhar**…**RV Nair,** V Balakrishnan - Advanced Optical Materials, 2026 **Abstract:** Defect-localized excitons in monolayer transition-metal dichalcogenides like WS_2, have attracted enormous interest due to their vast applications in optoelectronics and quantum technologies. Although chemically doped monolayers exhibit a defect-bound exciton, this distinct feature has preliminary been observed at cryogenic temperatures. Here, we report a prominent defect-bound excitonic state at room temperature (RT), about 130 meV below the characteristic exciton emission line, in Vanadium-doped WS_2 (V-WS_2) monolayers. Temperature-dependent differential reflectance spectra reveal the presence of defect-bound excitons from 4 K to room temperature. Furthermore, with increasing V-concentration, a gradual increase in binding energy is observed, from 106 meV at 1.2 wt.% V-WS_2 to 130 meV at 4 wt.% V-WS_2 in photoluminescence (PL). Temperature-dependent PL studies show the sharpening of defect-emission at low temperatures, from ~45 nm at RT to ~3 nm at 4 K. The time-resolved PL spectra reveal the increased PL decay lifetimes from 30 ± 0.4 ps in pristine WS_2 to 38 ± 0.6 ps in V-WS_2 at 20 K temperature, confirming the trap-states. We find that V-doping induces localized excitons, and increasing the vanadium concentration enhances the Coulomb interaction, stabilizing the defect emission at RT.
44.	Heterogeneous oblique double random forest **MA Ganaie,** M Tanveer, I Beheshti, N Ahmad, PN Suganthan - Neural Network, 2026 **Abstract:** The decision tree ensembles use a single data feature at each node for splitting the data. However, splitting in this manner may fail to capture the geometric properties of the data. Thus, oblique decision trees generate the oblique hyperplane for splitting the data at each non-leaf node. Oblique decision trees capture the geometric properties of the data and hence show better generalization. The performance of the oblique decision trees depends on the way oblique hyperplanes are generated and the data used for the generation of those hyperplanes. Recently, multiple classifiers have been used in a heterogeneous random forest (RaF) classifier. However, it fails to generate trees of proper depth. Moreover, double RaF studies highlighted that larger trees can be generated via bootstrapping the data at each non-leaf node and splitting the original data instead of the bootstrapped data recently. The study of heterogeneous RaF lacks the generation of larger trees, while the double RaF based model fails to take over the geometric characteristics of the data. To address these shortcomings, we propose a heterogeneous oblique double RaF. The proposed model employs several linear classifiers at each non-leaf node on the bootstrapped data and splits the original data based on the optimal linear classifier. The optimal hyperplane corresponds to the models based on the optimized impurity criterion. The experimental analysis indicates that the performance of the introduced heterogeneous double random forest is better than the baseline models. To demonstrate the effectiveness of the proposed heterogeneous double

	random forest, we used it for the diagnosis of Schizophrenia disease. The proposed model predicted the disease with higher accuracy compared to the baseline models.
45.	Hexagonal boron nitride with vacancy engineering as an efficient polysulfide anchor and electrocatalyst for Na–S batteries **M Kaur, TJD Kumar** - Nanoscale, 2026 **Abstract:** Sodium–sulfur (Na–S) batteries have become a major focus of research because they can supply large amounts of energy at a minimal cost, depending on the natural abundance of sodium and sulfur. Despite these benefits, their widespread application remains limited because of several persistent issues, particularly brought on by the significant capacity loss caused by the dissolution of sodium polysulfides (NaPs) and the intrinsically sluggish reaction kinetics connected to their electrochemical conversion. In this work, we systematically analyzed the impact of vacancy-induced modifications in hexagonal boron nitride (h-BN) that enhance its catalytic performance and its ability to anchor sulfur species. Density functional theory calculations indicate that pristine h-BN interacts weakly with NaPs. On the other hand, introducing vacancies significantly enhances the interaction strength. Single nitrogen and single boron vacancies substantially boost the adsorption, and even stronger binding is attained when double nitrogen or double boron vacancies are created, thus lowering the polysulfide shuttle. The promise of vacancy-engineered h-BN as an efficient anchoring material is further demonstrated by the polysulfides' stronger binding to vacancy-engineered sheets compared to electrolyte molecules. The density of state calculations demonstrate that the h-BN lattice's electrical characteristics are much improved by the creation of vacancies, changing it from an insulating material to one with semiconducting or even semimetallic behavior. Overall, our results provide fundamental insights and demonstrate that vacancy-engineered h-BN is an excellent host material for reducing the shuttle effect in Na–S batteries because of its favorable electronic properties, structural robustness, and strong affinity for NaPs species. 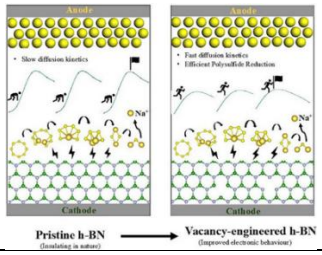
46.	HiT-HGR: A multi-scale oriented hierarchical transformer for hand-gesture recognition S Narayan, M Verma, P Hambarde, **SK Vipparthi,** S Murala, M Abdel-Mottaleb - IEEE MultiMedia, 2026 **Abstract:** Hand gestures play a crucial role in human-computer interaction, aiding applications like sign language interpretation, autonomous vehicles, and virtual reality. However, designing effective hand gesture recognition (HGR) systems remains challenging due to issues such as cluttered backgrounds and occlusion. This paper proposes a multi-scale oriented hierarchical vision transformer (HiT-HGR) framework, which targets extracting local and global receptive information for HGR from raw images. The HiT-HGR framework includes multi-scale feature assimilator (MSFA) to extract fine to coarse exquisite features with its multi-scale assimilation and a three-fold attention network (TFAN) to capture local to global dependencies. Cohesively, MSFA and TFAN allow the HiT-HGR framework to compile refined low-level to high-level features by considering local to global dependencies. Thus, the resultant features focus on only gesture features, ignore the background complexities, and enhance the performance of HGR. Extensive experiments demonstrate that the HiT-HGR framework outperforms conventional vision transformer models, and state-of-the-art HGR methods.

47.	Impact of wetting and drying cycles on reclaimed asphalt pavement and warm mix asphalt performance: Comparison with long-term aging conditions for pavement durability K Monu, **SK Sahdeo,** GR Rongaimei Naga - Journal of Transportation Engineering, Part B: Pavements, 2026 **Abstract:** The primary objective of this study was to evaluate the effect of reclaimed asphalt pavement (RAP) and warm mix asphalt (WMA, Sasobit) combinations on moisture susceptibility, fatigue resistance, rutting behavior, Marshall stability, and aging of bound base-course mixes. Two RAP sources (from pavements with different service lives) were incorporated at ≈35% and ≈70% by mix mass, and mixtures were produced as hot mix asphalt (HMA) and WMA. Specimens were conditioned under two environmental regimes' standardized long-term aging (LTA) and accelerated alternate wetting–drying (W&D) cycles and tested for Marshall stability, indirect tensile strength (dry/wet), rutting resistance (dynamic stability), and fatigue life (four-point bending). Alternate W&D cycles produced measurable degradation: fatigue life declined by roughly 10%–21% (dependent on RAP content); and moisture resistance (indirect tensile ratio) decreased by about 4%–9% in several WMA cases. LTA tended to increase stiffness and Marshall stability but did not reproduce the same moisture-driven losses observed under W&D. The results indicate a trade-off: WMA with Sasobit improves workability and can reduce some aging-related losses at moderate RAP contents, yet lower mixing/compaction temperatures may limit RAP–virgin binder blending and increase moisture vulnerability unless antistripping measures are applied. Therefore, WMA is a promising option for RAP-inclusive mixes when moisture risk is managed. It should not be adopted unconditionally in moisture-prone environments.
48.	Improved soil moisture classified maps from fusion of optical and microwave satellite datasets R Kaur, R Maini, **RK Tiwari** - Journal of the Indian Society of Remote Sensing, 2026 **Abstract:** Soil moisture (SM) is a critical component in the fields of plant growth, soil health, climate and weather forecasting, erosion management and water resource management. The continuous monitoring of SM allows enhancement of crop yield and food security. Remote sensing is a state-of-the-art technology to measure the SM globally in an efficient way without any major financial requirements. The integration of two distinct types of electromagnetic radiation i.e., optical and microwave, ensures all-weather and accurate SM monitoring. However, the classification of fused datasets remains a challenging task due to the difficulty in preserving spectral and spatial information. In this article, different image fusion methods i.e., (a) nearest neighbour diffusion (NND), (b) gram Schmidt (GS), and (c) principal component analysis (PCA) have been implemented to develop SM maps using various classifiers i.e., (a) Multilayer Perceptron (MLP) based neural network (NN), (b) support vector machine (SVM), and (c) random forest (RF). To implement these algorithms, two global-level satellite datasets i.e., MODIS along with SCATSAT-1, were utilized over a part of North Indian. The performance analysis confirmed the efficacy of NND and ANN in the development of improved SM maps with an accuracy of 94.14%. This outcome of the study allows the precision SM monitoring which directly impacts the economy, ecosystem sustainability and food protection.
49.	Influence of ceramic retention on inter-splat bonding and mechanical behavior of cold-sprayed Cu-ZrC composite coatings **SW Khan,** G Vidla, **KLSS Vasu,** A Ganvir, **E Singla, H Singh -** Materials & Design, 2026 **Abstract:** Cold-sprayed metal-ceramic composite coatings offer a promising route for high-performance surface engineering; however, the influence of ceramic retention on inter-splat bonding and mechanical performance remains insufficiently understood. In this study, Cu-ZrC composite coatings containing 30–85 wt% ZrC were deposited on Al-6061 substrates to

	investigate deposition behavior, interfacial integrity, and tribological response. Coating build-up was achieved for all compositions, although deposition efficiency decreased at higher ceramic loading due to increased particle rebound and reduced matrix continuity. Hardness increased continuously with ZrC content, while adhesion strength and scratch resistance showed non-linear behavior, with optimum cohesion observed at intermediate compositions (50–70 wt% ZrC). Scratch testing revealed reduced penetration depth and improved resistance to localized deformation with increasing ceramic content, indicating enhanced inter-splat bonding. Ball-on-disk wear testing demonstrated a progressive reduction in wear volume, reaching ~ 93% lower wear for the 85 wt% ZrC coating compared to pure Cu, accompanied by a transition from ductile adhesive wear to brittle fragmentation-dominated mechanisms. Overall, intermediate ceramic contents provided the best balance between deposition efficiency, mechanical integrity, and tribological performance. 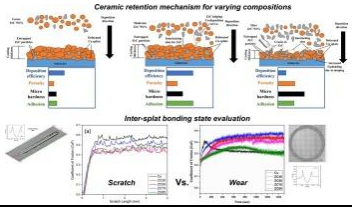
50.	Influence of high-energy ball-milling on the rheological properties of molded ultra high molecular weight polyethylene and its correlation with the structural alteration CK Raul…**C Sasmal,** SS Banerjee - Polymer Engineering & Science, 2026 **Abstract:** In this work, the influence of high-energy ball-milling on the rheological properties of molded ultra-high molecular weight polyethylene (UHMWPE) was explored and correlated with its structural alterations. The effect of ball-milling on material properties was primarily analyzed through shear rheology. Notably, both shear and absolute value of complex viscosities decreased by more than 10 orders of magnitude with increasing ball-milling time; however, the rate of reduction becomes less pronounced beyond 30 min of milling. Linear viscoelastic measurements and time-temperature superposition (TTS) studies revealed a distinct shift from a reptation-dominated terminal region and rubbery plateau to a Rouse-dynamics-dominated high-frequency transition region in the 30min ball-milled specimen compared with the neat UHMWPE. This transition suggested a decrease in entanglement density and the formation of shorter chains due to chain scission. This is further supported by a significant increase (greater than sevenfold) in the molecular weight between entanglements for the 30 min ball-milled specimen compared with the neat one. Microstructural evidence revealed that the particle morphology evolves from initially spherical to lamellar and flake-like structures, resulting from particle flattening and chain interdiffusion during milling, followed by delamination and fragmentation. In addition, X-ray diffraction analysis indicated the evolution of a prominent monoclinic phase following ball-milling. Thermal analysis revealed a slight decrease in crystallinity from ~59% for neat UHMWPE to ~51% after 30 min of milling. Dynamic mechanical analysis further supports the rheological findings, demonstrating a reduction in storage modulus and overall stiffness, which is attributed to decreased entanglement density and possible chain shortening.
51.	Insights into lithium-germanium interface dynamics in HPGe detector: A GEANT4 study **S Devi, K Tiwari, SS Kaintura, PP Singh** - Nuovo Cimento della Societa Italiana di Fisica C, 2026 **Abstract:** The performance of High-Purity Germanium (HPGe) detectors is strongly affected by dead layer characteristics, which modify charge collection and cause γ-ray attenuation. Energy loss in these regions is particularly significant at low photon energies, where absorption reduces Full Energy Peak Efficiency (FEPE), while the effect becomes less pronounced at higher energies.

	Since dead layer parameters are often unspecified by manufacturers, independent characterization is essential for accurate efficiency determination. In this work, the simulation of dead layer effects on a coaxial p-type HPGe detector, encapsulated in radiopure carbon fiber housing, was studied using various energies through GEANT4-based Monte Carlo simulations. The comparison of simulation with experimental data yielded an optimized top dead layer thickness of 0.72 mm.
52.	Interface-driven performance enhancement in perovskite solar cells using oxygen-tuned Cu-doped NiO_x hole transport layer **Puja,** PK Bhunia, **A Verma, G Bassi,** MAG Namboothiry, **M Kumar** - Solar RRL, 2026 **Abstract:** This work presents detailed investigation of defect chemistry and interface quality-driven performance enhancement of oxygen-tuned Cu-doped NiO hole transport layer (HTL) for perovskite solar cell (PSC). The results revealed that an increase in oxygen partial pressure activated dramatic variations in stoichiometry and electrical properties of Cu-doped NiO. The HTL layer prepared at 20% PO_2 during the growth showed the highest conductivity with a value of 12.9 S/cm, while the 10% PO_2 HTL exhibited the highest fraction of Ni^{3+} (0.76). Energy band alignment of HTL with perovskite layer demonstrated a minimal valence band offset of 0.13 eV for 20% PO2, which favors the efficient hole transfer between the two layers. Controlled oxygen partial pressure in HTLs reduces defect density from a peak of 3.01×10^{11} cm^{-3} at 10% PO_2 to 1.71×10^{11} cm^{-3} at 20% PO_2 and led to a twofold enhancement in the charge extraction rate. Finally, PSC based on the optimum HTL significantly boosts the efficiency with the power conversion efficiency reaching to 13.7% while reducing hysteresis to 4.5% from 7.60% in the controlled sample. This work links O_2 partial pressure-controlled defect chemistry and Ni^{3+}/Ni^{2+} ratio in inorganic HTLs to interfacial band alignment and device performance.
53.	Ion flux-induced effects on the nanoscale morphology of poly(dimethylsiloxane): Implications for tunable SERS response **P Kumar, J Singh, S Sarkar** - ACS Applied Nano Materials, 2026 **Abstract:** Micro and nanoscale patterning of polymeric surfaces has attracted considerable interest due to its relevance in flexible electronics, biosensing devices, optical components, and surface-enhanced Raman scattering (SERS) substrates. We investigate the evolution of nanoscale surface morphology in polydimethylsiloxane (PDMS) under low-energy ion irradiation, focusing on the role of ion flux. While ion-beam-induced patterning in polymers has been widely studied, the flux-dependent mechanisms governing stress generation and wrinkle formation at the nanoscale in PDMS remain largely unexplored. Our results reveal a strong flux dependence in surface morphology and wrinkle development. At lower beam currents, corresponding to ion fluxes $\sim 10^{14}$ ions cm^{-2} s^{-1}, longer irradiation times allow viscoelastic relaxation and radical recombination, thereby limiting compressive stress buildup and producing weakly developed wrinkles. In contrast, higher beam currents, corresponding to ion fluxes $\sim 10^{15}$ ions cm^{-2} s^{-1}, promote rapid ion-induced surface stiffening, enabling efficient compressive stress accumulation and the formation of well-defined wrinkle patterns. In contrast, crystalline Si irradiated under identical conditions shows negligible surface morphological evolution, underscoring the fundamentally different response of polymeric and crystalline materials. Nanomechanical measurements reveal a clear increase in the Young's modulus of the irradiated surface layer, from 1.5 MPa (pristine) to 11 MPa upon irradiation indicating progressive stiffening with ion exposure. Complementary X-ray photoelectron spectroscopy confirms the formation of a silica-like SiO_x layer confined within the ion penetration depth, establishing the chemical origin of the mechanical modification. Finally, SERS measurements on the patterned surfaces show a systematic dependence of enhancement, albeit small, on beam current, demonstrating that ion-beam-driven morphology control provides a versatile route to engineer functional nanostructured SERS-active polymer substrates.

	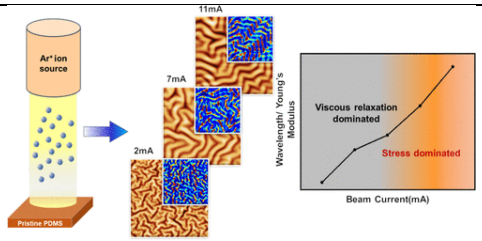
54.	Isolation, characterization, and proof of concept evaluation of serially adapted bacteriophages against multidrug-resistant escherichia coli **V Rathi**…**A Poundarik** - Folia Microbiologica, 2026 **Abstract:** This study was conducted to test serially passaged bacteriophages for combating multidrug-resistant *Escherichia coli* strains and to address the urgent need for sustainable alternatives to antibiotics. Bacteriophages were isolated from diverse environmental sources against *E. coli* MTCC 1687. All bacteriophages were sequentially passaged for adaptation against three multidrug-resistant (MDR) strains, *E. coli* (R1, R2, and R4), with host efficiency expansion measured by efficiency of plating (EOP). Two phages (VR1 and VR4*) were selected based on their in vitro lytic, antibiofilm activity, and live-dead analysis. Both phages were characterized for adsorption kinetics, one-step growth parameters, pH tolerance, and thermal stability. A proof-of-concept in vivo study was conducted with a two-phage (VR1 and VR4*) cocktail. Phages were orally delivered in drinking water to one-week-old chickens 24 h after an intraperitoneal challenge with MDR *E. coli* R4. Bacteriophages exhibited significant lytic and antibiofilm activity in a dose-dependent manner. Short latent periods of 10 min (VR1) and 15 min (VR4*), stability > 50% at pH ≥ 4, when formulated in a stabilizing buffer, and thermal stability at room temperature were observed in the bacteriophages. In the proof-of-concept study of a controlled chicken infection model using a resistant *E. coli* strain, an orally administered two-phage cocktail (VR1 and VR4*) achieved 100% survival over a 7-day observation period. Lesion severity and histopathological outcomes were comparable to those of antibiotic treatment. This research established a proof-of-concept for host-adapted bacteriophages as adaptable and potent antimicrobial agents against field-isolated multidrug-resistant strains. The findings provide preliminary support for developing a phage platform to improve animal health, food safety, and, ultimately, human health.
55.	Label-free chemiresistive biosensor for breast cancer specific point mutation detection in BRCA-1 gene **D Singh, M Sharma, B Das, S Tripathy** - IEEE Sensors Letters, 2026 **Abstract:** Breast cancer remains the most prevalent malignancy among women worldwide, with incidence rates continuing to rise due to multiple genetic and environmental factors. Among these, the 185delAG mutation in the BRCA1 gene is strongly associated with impaired DNA repair mechanisms and increased cancer susceptibility. In this study, a label-free chemiresistive biosensor platform is presented for the detection of the BRCA1 185delAG mutation. The proposed sensor employs conductive solid and hollow polyaniline (S&H-PANi) nanofibers as the sensing layer, forming a conductive bridge across gold interdigitated electrodes. Surface immobilization of 5' NH2-modified single stranded probe DNA is achieved via glutaraldehyde as crosslinker on PANi nanofibers, enabling selective hybridization with complementary target DNA sequences. The sensing mechanism is based on changes in electrical resistance arising from negative charge accumulation on the PANi matrix upon DNA hybridization, which modulates the conductivity of the nanofiber network. Sensor performance is evaluated by monitoring the change in resistance (ΔR) upon target hybridization, as a function of the target dose (1 pM – 0.01 μM). Comparative analysis reveals that hollow PANi nanofibers exhibit higher sensitivity than solid nanofibers, attributed to enhanced surface accessibility and charge interaction. Specificity studies conducted using complementary (C26), mismatched (M26), and non-target (Blank PBS) samples confirm the

	sensor's ability to discriminate specific mutations with high fidelity. The developed platform offers a rapid, cost-effective, and portable solution for genetic mutation detection, highlighting its potential for integration into point-of-care diagnostic applications.
56.	Metaheuristic-optimized bell-shaped slotted pentaband patch antenna for C, X, Ku, and K band applications M Hannan, A Singh, **S Bansal,** F Shafi, O Singh, M Aknan, K Kouser - Scientific Reports, 2026 **Abstract:** The current study proposes a compact metaheuristic optimization-driven design of the slotted pentaband patch antenna with a bell-shaped patch, operating in the C, X, Ku, and K bands for satellite telemetry, radar sensing, and wideband transceivers. The antenna structure comprises a bell-shaped patch with C-slots, tilted vertical edges, and three semicircular perturbations on the horizontal edge of the patch to excite several resonant modes, mainly TM10, TM11, and TM20, with uniform surface current distribution. The antenna has five resonant frequencies at 5.2, 8.4, 10.4, 12, and 19.2 GHz with a reflection coefficient of less than -15 dB and maximum antenna gains of 8.83 dB, 4.96 dB, 7.87 dB, 6.13 dB, and 6.37 dB at the corresponding resonant frequencies. The antenna also has maximum radiation and total efficiencies of at least 85% in the C and X bands and above 95% in the Ku and K bands. In addition, the antenna performance is improved using five different metaheuristic optimization techniques, and the optimal results are obtained using the multi-objective optimization technique. Among the optimization techniques, the performance of the Differential Evolution (DE) algorithm is found to be the best, with improvements of up to 4.0% in S11, 2.2% reduction in VSWR, and improvements in antenna gains and efficiencies of up to 0.7%. The proposed antenna design using the electromagnetic simulator, circuit simulator, and optimization tools provides the best platform for the proposed antenna and is further validated experimentally.
57.	Modified end bonding of cross-bonded cables terminated at non-uniform minor sections **A Das, CC Reddy** - IEEE Transactions on Power Delivery, 2026 **Abstract:** This letter presents a novel end-bonding method for cross-bonded High Voltage power cables with non-uniform minor section lengths, a practical scenario not addressed in IEEE Std. 575. In cable rerouting applications, unequal section lengths lead to severe circulating screen currents and overvoltages. To overcome this limitation, a novel end-bonding scheme is proposed to suppress screen current and voltage. The test results demonstrate that the proposed method outperforms conventional direct grounding and grounding with a screen voltage limiter under both steady-state and transient conditions.
58.	Multidirectional spin–orbit torque magnetization dynamics in beyond room temperature van der waals magnet devices B Zhao, **L Bainsla**…SP Dash - Nano Letters, 2026 **Abstract:** van der Waals (vdW) magnets with room-temperature ferromagnetism offer exciting opportunities for energy-efficient spintronic devices, yet their magnetization dynamics remain largely unexplored despite their importance for high-speed memory technologies. Here, we investigate spin–orbit torque phenomena in the room-temperature vdW magnet $(Co_{0.15}Fe_{0.85})_5GeTe_2$ (CFGT)/Pt heterostructure using spin-torque ferromagnetic resonance and second-harmonic Hall measurements. Alongside a conventional in-plane spin Hall conductivity of 3.68×10^5 $(\hbar/2e)$ $(\Omega\ m)^{-1}$, we identify a sizable out-of-plane component of -0.33×10^5 $(\hbar/2e)$ $(\Omega\ m)^{-1}$ that generates unconventional damping-like torques. Density functional theory and Monte Carlo simulations suggest that this torque can originate from interface-induced spin reorientation arising from a modified magnetic anisotropy landscape and strongly enhanced Dzyaloshinskii–Moriya interaction at the CFGT/Pt interface. The combination of low effective magnetization

	(0.321 T), moderate Gilbert damping (0.027), and efficient multidirectional torques highlights vdW magnets as promising platforms for next-generation spintronic devices. 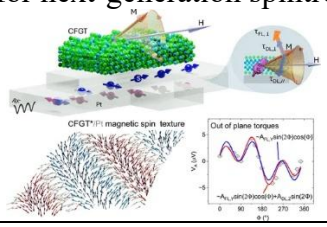
59.	Network structure shapes pollinator collapse under rapid shifts in demographic rates with random fluctuations **R Kumar K, PS Dutta** - Proceedings of the Royal Society B: Biological Sciences, 2026 **Abstract:** Ongoing environmental change threatens the persistence of species in ecological communities. Plant–pollinator mutualistic networks, which support biodiversity and ecosystem functioning, are particularly vulnerable to such disturbances. Although environmental variation is known to modify demographic rates and weaken mutualistic interactions, how its pace and stochasticity jointly affect the stability of mutualistic networks remains largely unknown. Here, we analyse a high-dimensional mutualistic network model with time-varying demographic rates, such as mortality and competition alongside noisy fluctuations. A reduced two-dimensional model reveals that sufficiently fast parameter change can trigger rate-driven pollinator collapse, which is further expedited by noise. These dynamics persist in the high-dimensional mutualistic network. Using 30 empirical plant–pollinator communities, we show that network structure is associated with vulnerability to rapid change in demographic parameters, as measured by critical rates: higher connectance and nestedness increase tolerance to rapid changes across noise intensities, whereas higher modularity reduces stability, leading to collapse at lower rates of change. Overall, our results highlight that the pace and variability of demographic changes interact with network structure to shape the stability and persistence of mutualistic communities.
60.	Numerical investigation of the flexural behaviour and composite action of reinforced concrete sandwich panels (RCSP) with EPS core: Parametric study using FEA **HK Kassa, P Haldar,** A Ahmad - Scientific Reports, 2026 **Abstract:** Conventional unreinforced brick masonry walls pose significant sustainability and seismic vulnerability challenges due to excessive resource consumption and self-weight. Reinforced Concrete Sandwich Panels (RCSP) with Expanded Polystyrene (EPS) core present a promising alternative, offering similar functional benefits while being lightweight, sustainable, and exhibiting enhanced seismic performance. This study investigates flexural behaviour of RCSP using validated three-dimensional nonlinear finite element model developed in Abaqus/Explicit, demonstrating close agreement with experimental results in terms of ultimate load capacity, crack initiation and propagation, and failure mechanisms. A systematic parametric study evaluated the influence of shear connector type, spacing, diameter, Welded Wire Mesh (WWM) size, EPS core thickness, and longitudinal reinforcement. Among connector types, Double-Truss Shear Connectors (DSC) increased the ultimate load capacity by up to 12–18% and improved post-peak ductility compared to orthogonal and Single-Truss Shear Connectors (SSC). Reducing connector spacing from 150 to 75 mm enhanced the ultimate load capacity by approximately 8.9%, with negligible change in failure mode. Increasing WWM diameter from 3 to 6 mm resulted in significant increase in flexural strength of up to 102.8%, indicating strong dependence on reinforcement stiffness. Variations in EPS core thickness showed less than 3% change in flexural capacity, confirming its negligible structural contribution under bending. Inclusion of additional longitudinal reinforcement (6 mm Fe500 bars at 160 mm spacing) increased ultimate load capacity by 40.5% and significantly enhanced ductility. These findings provide critical insights into the

	governing parameters affecting composite action and offer design-oriented recommendations for optimizing RCSP systems as lightweight, sustainable, and seismic-resilient alternatives to conventional masonry walls.
61.	Pepholin, a bacteriophage holin-derived antimicrobial peptide with membrane-disruptive activity and therapeutic efficacy in MDR pseudomonas aeruginosa burn wounds RV Purushotham…**A Kumar,** SK Singh, S Dandapat - RSC Advances, 2026 **Abstract:** The emergence of multidrug-resistant (MDR) *Pseudomonas aeruginosa* poses a serious threat to burn wound healing, necessitating the development of alternative therapeutics beyond conventional antibiotics. In this study, an artificial intelligence guided design strategy was employed to identify a novel antimicrobial peptide (AMP), Pepholin (12 amino acids, net charge +5) derived from the holin protein of a *Pseudomonas* bacteriophage, highlighting holins as an underexplored scaffold for AMP discovery. Pepholin demonstrated strong antibacterial and antibiofilm activities against MDR *P. aeruginosa*, achieving complete bacterial eradication within 90 minutes. Mechanistic investigations confirmed that Pepholin exerts its bactericidal action by permeabilizing bacterial membranes and disrupting membrane integrity in a concentration and time dependent manner. The peptide exhibited high hemocompatibility and minimal cytotoxicity in mammalian cells, resulting in selectivity indices greater than 8. Pepholin retained its antibacterial activity under physiological conditions of salt, serum, and temperature. To explore its therapeutic potential, Pepholin was incorporated into a carbomer-based hydrogel and evaluated in a murine burn wound infection model caused by MDR *P. aeruginosa*. Topical treatment significantly enhanced bacterial clearance, accelerated wound healing, promoted collagen deposition, and modulated cytokine responses. Collectively, these findings demonstrate that bacteriophage holin derived peptides represent a promising new class of antimicrobial agents and establishes Pepholin as a stable, biocompatible, and mechanistically defined AMP with dual antimicrobial and wound-healing activity, supporting its development as a next-generation therapeutic for infected wound management. 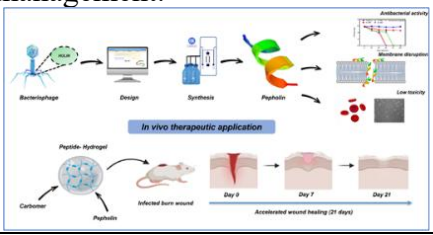
62.	PES2MP: A Python application for automating collisional dynamics of linear rigid-rotors **A Kushwaha, P Chahal, H Tatin, TJ Dhilip Kumar** - Journal of Computational Chemistry, 2026 **Abstract:** The paper introduces a modular Python-based program with a graphical user interface (GUI) to automate collisional dynamics of rigid-rotors in cold and ultracold environments. The program streamlines the construction of ab initio potential energy surfaces (PES), with optional neural network (NN) augmentation, thereby reducing computational costs. The multipole expansion module generates radial terms for Molscat to compute inelastic cross-sections and state-to-state rate coefficients. These rate coefficients, especially with hydrogen and helium, are crucial for determining column densities and modeling the abundances of species in the interstellar medium. In the paper, the rate coefficients of C2-He/H2 are calculated for the first 11 rotational states to evaluate the accuracy of the ab initio and NN methods. Finally, the rate propensities for Cn, HCn, HC−n, HC+n, and HCnN linear chains (n ≤6) are calculated based on the benchmark results and delivered as an ensemble NN model to allow the direct prediction of rate coefficients based on the physical parameters of various carbonaceous species. The GUI-automated PES generation/fitting accelerates collisional studies, ensures robustness and reproducibility, and

	significantly reduces data processing time from weeks to hours, thereby providing an efficient and general framework for accurate state-to-state rate predictions in astrochemical and molecular dynamics applications.
63.	Post-earthquake recovery of reinforced concrete buildings in India: Hybrid framework and application **D Baldev, M Surana** - Bulletin of Earthquake Engineering, 2026 **Abstract:** India, one of the world's most seismically active regions, has endured losses from earthquakes, underscoring the need for robust earthquake risk management. Existing post-earthquake recovery frameworks estimate repair costs and downtime using region-specific vulnerability/fragility functions and often overlook the socioeconomic and impeding factors. This study introduces a novel, hybrid framework to assess the post-earthquake recovery of reinforced-concrete moment resisting frames in India. The study integrates existing strain-based seismic damage estimation at component and building scales and quantifies repair cost, downtime, and recovery trajectories. Repair cost and downtime estimates are drawn from consultations with structural repair engineers and impeding factors derived from historical earthquakes. The framework is demonstrated on four- and eight-story reinforced-concrete moment-resisting frames with varying configurations under multiple recovery constraints. The results show that, for four-story moment resisting frames, mean repair costs are 8%, 11%, and 16% of replacement cost for 'minor', 'moderate', and 'severe' damage states, respectively, which increase to 11%, 16%, and 24% for eight-story moment resisting frames. Downtime estimates based on single-worker allocation per floor under parallel and sequential repair strategies range from 1.45–1.77 years ('minor') to 1.99–2.78 years ('severe') for four-story archetypes, and from 1.70–3.56 years ('minor') to 2.46–6.75 years ('severe') for eight-story archetypes, incorporating delays from inspections, mobilization, administration, and approvals. The proposed framework guides policymakers and engineers to assess and optimize earthquake preparedness and resilience in India, considering structural and socioeconomic dimensions of recovery.
64.	Prioritizing Industry 4.0 obstacles for the transition towards Industry 5.0 **C Dixit, R Kumar,** TU Daim - Technology in Society, 2026 **Abstract:** The global business transition to digitalisation is a technological shift and a triple-bottom-line development, involving data-driven decision making, influencing automation, flexibility, and sustainable development. A systematic literature review examines the obstacles that influence the adoption of Industry 4.0. These obstacles are categorized according to the Technology-Organization-Environment (TOE) framework. The interrelationships among these obstacles are studied using a novel methodology, the Decision-Making Trial and Evaluation Laboratory (DEMATEL), based on an interval-valued hesitant fuzzy (IVHF) linguistic approach. This study models the complex relationships among Industry 4.0 obstacles in an uncertain environment to simultaneously address hesitation, uncertainty, and interval imprecision in expert judgment. The results show that 1) ineffective knowledge management systems, insufficient digital and internet infrastructure, workforce skill gaps and limited collaborative research initiatives emerge as the significant obstacles that impact the readiness for Industry 4.0 technologies adoption; 2) using the concepts of hesitant IVHF the dominance of critical obstacles in the optimistic scenario and their exclusion in the pessimistic scenario indicate that these obstacles are condition-dependent. The significance of these obstacles will impact the adoption of Industry 4.0, particularly in specific environments. Policymakers, operations, and supply chain managers will benefit from this study, as it addresses the challenges of the transition towards Industry 4.0, and future studies will determine the pathway to Industry 5.0.
65.	Projected climate extremes and compound hydro-meteorological stressors across India based on CMIP6 multi-model ensembles

	M Singh, R Kumari, **S Pathak,** A Hussain - Theoretical and Applied Climatology, 2026 **Abstract:** Climate change is altering the occurrence, intensity and duration of extreme hydro-meteorological events that have a strong influence on the surface water systems. Although various direct inputs of pollution are often viewed as the main factors that lead to water-quality degradation, climate-based changes in temperature and precipitation become more and more basic stressors due to changes in thermal regimes, runoff processes, and dilution ability. This study assesses the CMIP6 multi-model ensembles based on historical (1981–2014) and four Shared Socioeconomic Pathways (SSPs) scenarios to assess future climatic extremes and compound hydrometeorological stressors in India. The influence of climatic variables on water-quality processes was examined by analysing variability in extreme precipitation intensity, dry spells, temperature extremes, diurnal temperature range (DTR), and their seasonal interactions. Results indicate robust warming effect in all the scenarios. Stronger nighttime warming leading to a consistent DTR decline of -1.6 to -2.2 °C by end-century. Dry spells are increased in several parts of the country with consecutive dry days (CDD) rising by 30–45 days by end century. The drastic rainfall occur during the monsoon and post-monsoon. Thermal restructuring by moisture is a prevailing hydrometeorological stressor reflected by the high seasonal correlation between precipitation and DTR suppression (r = -0.8 to -0.85 and $p < 0.01$). The frequency of compound hot-wet events shows a clear increasing tendency under SSP5-8.5 by the end of the century, raising the likelihood of episodic runoff loading and enhanced thermal stress. This study presents a climate diagnostic assessment of hydro-meteorological stressors relevant to surface-water vulnerability.
66.	RA scoreboarding: Return address stack protection in RISC-V **L Sharma, SJ Badri, N Goel** - Journal of Systems Architecture, 2026, **Abstract:** RISC-V processor cores range from lightweight embedded to full-featured general-purpose designs. Their open-source nature and growing popularity have accelerated adoption and introduced significant security vulnerabilities. Due to their In-Order and Out-Of-Order (OoO) execution, these cores are susceptible to attacks like Spectre, Meltdown, and classical buffer overflows. This work is particularly focused on threats to control flow, such as return address (*ra*) corruption and subsequent side-channel leaks. Exploits like Spectre-RAS and Stack-Based Buffer Overflow (SBFO) can enable severe attacks like Return-Oriented Programming (ROP). These attacks hijack a system's control flow to execute malicious instruction sequences, directly violating its Control-Flow Integrity (CFI). Modern RISC-V architectures commonly use hardware Return Address Stack (RAS) for *ra* prediction. We discovered that the RAS structure is vulnerable to the Spectre-RAS attack, in which a single incorrectly predicted *ra* can leak secret data through side channels. We addressed Spectre-RAS along with SBFO with a new RAS scoreboarding and extension mechanism. Our method assesses prediction confidence by calculating a dynamic Trustzone score (*TScore*) per *ra*, reducing speculation on low-confidence returns. Implemented on the Boom OoO RISC-V core and simulated in gem5, *TScore* delivered measurable improvements. *TScore* improves RAS security against *ra* pollution without affecting RAS prediction rate and maintaining it up to 99.99%, eliminating mispredictions in some benchmarks like bitcnts and crc of MiBench completely, while maintaining less than 2% overhead in CPI across most workloads. The FireSim framework, integrated with Chipyard, was used to evaluate the proposed design for FPGA-backed RTL execution along with Gem5-based speculative analysis. Linux-based MiBench workloads were executed on AWS EC2 F2 FPGA instances, using the Xilinx Virtex UltraScale+ VU47P platform as the target, enabling runtime characterization of speculative return behavior, frontend redirects, and speculative control flow activity. Despite the minor hardware overhead, the proposed mechanism is useful for out-of-order RISC-V systems, as demonstrated by FPGA synthesis and timing analysis.
67.	Reprogramming dendritic cells to overcome tumor-mediated immune suppression

	JA Malik - Frontiers in immunology, 2026 **Abstract:** Dendritic cells (DCs) are indispensable orchestrators of antitumor immunity, yet in solid tumors, they frequently undergo profound dysfunction, enabling immune evasion and cancer progression. Recent advances have uncovered unexpected roles of DC subsets in tumor antigen processing, cross-presentation, and immune regulation that were previously underappreciated. In this review, the paper discusses novel mechanisms driving DC impairment, including epigenetic reprogramming, metabolic remodeling, and tumor-derived suppressive networks that converge to skew DC function toward tolerance. It highlights cutting-edge strategies that actively reprogram dysfunctional DCs, such as transcription factor modulation, nanoparticle-based antigen delivery, neoantigen and tumor lysate pulsing, and *in vivo* induction of DC-like phenotypes from malignant or stromal cells. The paper provides a conceptual framework for restoring DC immunogenicity in the tumor microenvironment by integrating these mechanistic insights with translational innovations. This perspective consolidates emerging knowledge and identifies promising therapeutic avenues to enhance the efficacy of DC-based cancer immunotherapy.
68.	Risk premia and hedging role of gold in the ICAPM framework: Evidence from India **B Raina,** P Mukherjee, **S Bardhan** - Journal of Economics and Finance, 2026 **Abstract:** Based on the Intertemporal Capital Asset Pricing Model (ICAPM) framework, this study empirically evaluates the hedging effectiveness of gold through an asset pricing lens; it examines the pricing of intertemporal risk in the Indian equity market by incorporating gold as a potential state variable. Using daily data spanning 2005 to 2024 for NIFTY-50 stocks, we generate time-varying conditional covariances using the DCC-GARCH model. To account for cross-equation error correlation while imposing common slope coefficients across return equations, we employ a panel Seemingly Unrelated Regression (SUR) model. Findings reveal that conditional covariances between the market, gold, and treasury bills are all statistically significant, hence acting as priced risk factors within the ICAPM structure. Notably, gold exhibits a negative risk premium, thereby confirming its role as an intertemporal hedge. Conversely, the positive and statistically significant risk premia on the market and treasury bills reflect compensation for systematic risks and sensitivity to shifts in the investment opportunity set, respectively. The findings add to the existing literature by reaffirming gold's hedging properties in the Indian equity market, albeit from an asset pricing perspective by assessing its risk premium. The study offers meaningful policy insights, especially in promoting gold as a financial instrument through regulated investment channels in India's financial landscape.
69.	Scatterometer and multispectral-based image pansharpening for improved spatial resolution snow cover maps R Kaur, **Sartajvir Singh,** GK Sethi - Remote Sensing Applications: Society and Environment, 2026 **Abstract:** Snow cover monitoring in the Western Himalayan region is essential for understanding regional climate variability, hydrological processes, and water resource management. This study investigates changes in snow cover using the integration of optical and microwave satellite datasets. Data obtained from MODIS (Moderate Resolution Imaging Spectroradiometer) and SCATSAT-1 (Scatterometer Satellite-1) were combined to improve the reliability of snow mapping in complex mountainous terrain. To enhance spatial detail and reduce the limitations of individual datasets, five pan-sharpening techniques—Brovey Transform (BT), Gram–Schmidt (GS), Intensity Hue Saturation (IHS), Nearest Neighbor Diffusion (NND), and Principal Component Analysis (PCA)—were applied before classification. Snow and non-snow areas were identified using the Support Vector Machine. The integration of microwave backscatter with optical reflectance improved the discrimination between snow and non-snow surfaces and

	enhanced the spatial clarity of the imagery. The results demonstrate that pan-sharpened images provide better boundary delineation and more reliable classification compared to optical data alone. Change detection analysis highlights variations in snow distribution across the Himalayan region. The findings confirm that the fusion of microwave and optical satellite data significantly improves snow cover mapping, particularly under cloud cover, and provides a reliable approach for monitoring snow dynamics in mountainous regions.
70.	Serum TP53 autoantibodies as a non-invasive diagnostic biomarker for canine mammary tumours: Comparative insights from human and experimental rat model P Kumar…**A Kumar** - Molecular Biology Reports, 2026 **Abstract:** Background Canine mammary tumours (CMTs) represent a valuable spontaneous model for human breast cancer, as both share comparable pathological features and frequent alterations in the TP53 pathway. Although TP53 involvement in tumour development is well established, the diagnostic relevance of circulating TP53 autoantibodies in dogs remains insufficiently characterized. This study evaluated the diagnostic utility of TP53 autoantibodies in CMTs using a recombinant TP53-based immunoassay, supported by comparative analyses in human and experimental animal models. Methods and Results Recombinant canine TP53 protein was expressed and employed in indirect ELISA and dot blot assays to detect serum TP53 autoantibodies in 141 canine serum samples, including sera from dogs with mammary tumours and healthy controls. Comparative evaluation included serum samples from 100 human subjects (50 breast cancer patients and 50 healthy individuals) as well as a longitudinal N-nitroso-N-methylurea (NMU)–induced rat mammary tumour model to examine the temporal appearance of autoantibodies before and during tumour development.TP53 autoantibodies were detected in 60.0% of dogs with mammary tumours and were absent in healthy controls ($p < 0.0001$), demonstrating high diagnostic accuracy (AUC 0.9587; sensitivity 60%; specificity 100%). Comparable trends were observed in human breast cancer sera (AUC 0.8956; sensitivity 52%; specificity 98%). Notably, longitudinal analysis of the NMU-induced rat model revealed the presence of TP53 autoantibodies before overt tumour formation, highlighting their potential role in early cancer detection. Conclusions These findings support recombinant TP53-based ELISA as a sensitive, specific, & non-invasive diagnostic approach and identify circulating TP53 autoantibodies as promising early biomarkers in comparative and translational oncology. 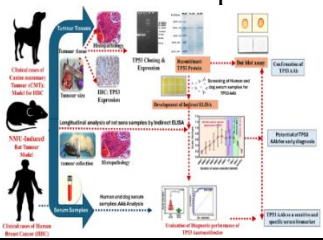
71.	Si-modified beta-Ti-25Mo biomaterials with reduced elastic modulus, enhanced corrosion resistance, and cytocompatibility **K Kumar, M Kamboj, B Das, H Singh, K Rakha** - Biomedical Physics & Engineering Express, 2026 **Abstract:** One of the key challenges for β-Ti alloys in biomedical applications is achieving a balance among low elastic modulus, high corrosion resistance, and cytocompatibility. In this study, Ti25MoxSi alloys (x = 0–2 wt.%) were designed to ensure a metastable β-phase. The alloys were fabricated using vacuum arc melting. Their microstructures and surfaces were evaluated by optical microscopy and XRD to assess the constituting phases. The elastic modulus and hardness of the alloys were evaluated using nanoindentation. The corrosion behavior in aerated Ringer's solution using Electrochemical analysis. SEM, MTT assay, and live/dead cell assay were used to examine the *in vitro* biological responses of all alloys. Optical microscopy shows equiaxed β-Ti grains in

	all alloys, with ultrafine silicide precipitates at grain boundaries in 1.5 and 2 wt.% Si content. XRD analysis reveals stable β-phase for all alloys. The nanoindentation studies show a reduced elastic modulus of 80–85 GPa. A significant enhancement in hardness was observed with typical values around 4 GPa. Preliminary electrochemical studies show improved corrosion resistance, suggesting the formation of a passive film upon adding Silicon. *In vitro* studies using MC3T3-E1 cells confirm cytocompatibility across all compositions. The study highlights the potential of Ti–Mo–Si alloys for load-bearing biomedical implants.
72.	Spatially correlated disorder in butterfly wing scales for enhanced light emission and absorption **M Aleem, K Singh, A Choudhary, RV Nair -** Journal of the Optical Society of America B: Optical Physics, 2026 **Abstract:** We investigate the multifunctional optical response of female Papilionoid butterfly wing scales, which have spatially distinct photonic environments that enable emission control and near-perfect light absorption. Atto 633 dye molecules embedded in the white crescent regions of wing scales exhibit modification of spontaneous emission rate with a ~ 2.6-fold reduction in emission lifetime. Lifetime reduction is attributed to the local photonic environment, which acts as effective nano-cavities like scattering regions in the wing scale morphology. The two point correlation function and fast Fourier transform analysis reveal short-range correlations that enable these nano-cavities (sub-micron holes) in white wing scales. However, the black region surrounding the white crescents displays extremely low reflectance, which functions as a near-perfect broadband absorber. The measured total and specular reflectivity spectra demonstrate absorption as high as 98% across the visible range. We use a finite-difference time domain simulation model based on realistic wing geometry to corroborate experimental observations along with wavelength-dependent Poynting vector distribution. Our results establish that the butterfly wing scales are capable of simultaneously modifying the emission rate and achieving near-perfect absorption, offering inspiration for nature-inspired strategies to design multifunctional nanophotonic devices.
73.	SPRTN preserves RNA polymerase I transcription under genotoxic drug stress in lung adenocarcinoma **M Sharma,** S Karnati, S Ergün, **S Naidu** - Frontiers in Oncology **Abstract:** Background: Hyperactivated RNA polymerase I (Pol I)-driven ribosomal DNA (rDNA) transcription sustains malignant growth and chemotherapy tolerance in lung adenocarcinoma (LUAD). Genotoxic chemotherapeutics such as doxorubicin and cisplatin preferentially damage rDNA by inducing DNA-protein crosslinks (DPCs), yet how tumor cells preserve Pol I transcriptional output under this damage remains poorly understood. Methods: We investigated SPRTN function in LUAD using complementary approaches spanning molecular, cellular, and in vivo levels, including DNA-protein crosslink isolation, chromatin immunoprecipitation, nascent RNA synthesis assays, apoptosis and invasion assays in SPRTN loss- and gain-of-function cell models, mouse xenograft studies, and transcriptomic analysis of clinical LUAD datasets. Results: SPRTN was enriched at the rDNA promoter, limited basal DPC accumulation, sustained Pol I transcriptional output, suppressed the p53-p21 nucleolar stress checkpoint, and promoted Pol I-dependent proliferation. Under doxorubicin or cisplatin treatment, SPRTN was recruited to G-quadruplex-rich rDNA promoters, a process associated with PARP-1 co-recruitment, and facilitated DPC resolution and transcriptional recovery. Catalytically inactive SPRTN failed to resolve rDNA-DPCs and restore Pol I output under both basal and drug-treated conditions. Doxorubicin- and cisplatin-resistant LUAD cells exhibited elevated SPRTN expression and enhanced rRNA synthesis relative to parental cells. SPRTN knockdown increased apoptotic response to doxorubicin and cisplatin, and co-inhibition of SPRTN and Pol I additively induced apoptosis in both parental and resistant cells. SPRTN further promoted Pol I-dependent migration

	and invasion. Transcriptomically, SPRTN was upregulated in LUAD, correlated with advanced disease stage and reduced overall survival, and was transcriptionally activated by ZEB1 and post-transcriptionally repressed by miR-195-5p. In vivo, SPRTN silencing reduced tumor burden and suppressed Pol I transcription, with further reduction upon doxorubicin treatment. Conclusion: These findings establish SPRTN as an rDNA-associated repair factor that couples genotoxic damage resolution to Pol I transcriptional resilience, defining the SPRTN-Pol I axis as a determinant of nucleolar homeostasis and therapeutic vulnerability in lung adenocarcinoma.
74.	Squeezing-fueled quantum otto engine via measurement-induced cooling: The two-qubit quantum rabi model **SR Rathnakaran, A Biswas -** Quantum Science and Technology, 2026 **Abstract:** We investigate a quantum Otto engine (QOE) constructed from the two-qubit quantum Rabi model, operating within a cavity quantum electrodynamics (QED) architecture. The engine operates with two qubits as the working substance and a single non-Markovian hot thermal bath, modeled via the hierarchical equations of motion formalism. In place of a conventional cold thermal reservoir, the cooling stroke is realized through a projective measurement protocol on the cavity mode, which acts as an ancillary subsystem and effectively mimics a cold bath for the qubit working medium via measurement back-action. A squeezing drive applied to the cavity mode serves as a quantum fuel. We demonstrate that cavity squeezing systematically enhances both the power output and operational efficiency of the engine—the work extracted per unit of heat drawn from the hot bath-driving it above the standard quantum Otto limit. In the limit-cycle regime, the efficiency, while remaining above the Otto bound throughout, asymptotically converges to it from above. This identifies squeezing as a controllable quantum resource for thermodynamic optimization. Our results reveal that the interplay between qubit–cavity coupling, measurement-induced cooling, and non-equilibrium squeezing gives rise to a multi-resource thermodynamic architecture with performance characteristics inaccessible to conventional two-bath QOEs, thereby providing a concrete route toward experimentally realizable quantum heat engines in cavity QED platforms.
75.	Stability and computational assessment of fractional Maxwell–Casson fluid in a Darcy-Brinkman model with variable porosity S Bansal, **AK Gupta,** S Sharma - International Journal of Numerical Methods for Heat & Fluid Flow, 2026 **Abstract:** Purpose Motivated by diverse industrial applications involving viscoelastic fluids in porous media, the current study aims to investigate the buoyancy-driven flow and heat transfer of Maxwell–Casson fluid over a vertical flat plate embedded with porous structures. Design/methodology/approach To account for flow resistance and permeability effects, the Darcy–Brinkman model with spatially varying porosity is adopted to characterize the transport within the porous medium. The fluid formulation enables accurate representation of non-Newtonian effects, where yield stress significantly influences both velocity and temperature profiles. Temporal linear stability analysis of the proposed model is conducted to investigate the dynamic response of the system under small perturbations. The governing fractional equations are discretized using a finite difference scheme in conjunction with the L1 algorithm, while the stability of the numerical procedure is validated through von Neumann analysis to ensure robustness of the computed results. The resulting flow and thermal fields are analyzed graphically, with comprehensive discussion provided to interpret the impact of key parameters. Findings Stability analysis of the system reveals that increasing the value of Casson fluid parameter () enhances the stability of the convective flow, whereas higher fractional order parameters (,) reduce stability by weakening memory-induced damping effects. Moreover, higher fractional orders lead to thicker velocity and thermal boundary layers accompanied by reduced heat diffusion. Collectively, these findings provide valuable

	insights for the design and optimization of porous media systems involving complex non-Newtonian fluids, offering practical guidance for effectively controlling heat and fluid transport in engineering applications. Originality/value The present work represents a novel contribution by developing a comprehensive framework for analyzing buoyancy-driven flow of viscoelastic fluids in porous media under a fractional-order framework. A key feature of this approach is its robustness and generality, achieved through the integration of the Maxwell–Casson fluid model with the Darcy–Brinkman model and variable porosity. The formulation effectively captures memory effects and yield stress behavior without requiring restrictive assumptions, while the adopted numerical scheme ensures stable and accurate solutions across varying physical parameters, making the model adaptable to a wide range of engineering thermal systems.
76.	Stereoselective dearomative formal [3+ 2] cycloaddition of indole with allenols: Access to structurally diverse cyclopenta [b] indoles **AC Shaikh, K Kaur, P Singh, RD Thombare,** AK P, MV Mane - Chemical Science, 2026 **Abstract:** Dearomative cycloaddition reactions of indoles offer a powerful strategy for rapidly increasing molecular complexity, yet intermolecular variants that proceed with high regio-and diastereocontrol remain uncommon. Herein, we report an iron(III) chloride-mediated dearomative formal [3+2] cycloaddition of indoles with arylsulfonyl allenols, providing direct access to densely functionalized cyclopenta [b]indoles with excellent diastereoselectivity. The reaction proceeds under mild Lewis acidic conditions without the use of precious metal catalysts and displays broad substrate scope, tolerating diverse substitution patterns on the indole core and allenols, including electron-rich, electron-deficient, sterically hindered, and fused systems, affording the desired tricyclic scaffold in moderate to excellent yields. The synthetic utility of this protocol is demonstrated through late-stage functionalization of pharmaceutically relevant indole-containing molecules, Double Cascade Dearomative Cycloaddition, gram-scale synthesis, and downstream product diversification. Mechanistic studies, including DFT energy calculation and isotopic labeling experiments, support an ionic, non-radical pathway involving Lewis acid activation of the allenol to generate a transient electrophilic intermediate, followed by a dearomative cyclization. This operationally simple and sustainable method enables rapid construction of structurally complex, nonplanar cyclopenta[b]indole frameworks of potential relevance in medicinal chemistry.
77.	Strength, durability, and microstructural characterization of alccofine-stabilized coal and incinerated bottom ash for highway infrastructure A Kumar, S Govindan, **A Santhosh** - International Journal of Pavement Research and Technology, 2026 **Abstract:** Coal bottom ash (CBA) from thermal power plants and municipal solid waste incinerated bottom ash (IBA) from waste-to-energy plants are produced in large volumes, creating critical disposal and environmental challenges worldwide. This study evaluates their feasibility for pavement applications by stabilizing them with ALCCOFINE 1108, an ultrafine, highly reactive supplementary cementitious material. Laboratory investigations including compaction, unconfined compressive strength (UCS), California Bearing Ratio (CBR), and durability tests were performed, supported by SEM and FTIR analyses. Untreated ashes exhibited inadequate strength for direct use in pavement layers. Stabilization, however, substantially enhanced their performance: at 28 days, UCS values increased to 925.8 kPa for CBA and 3859.2 kPa for IBA at 8% ALCCOFINE, with IBA achieving nearly fourfold higher strength. Durability tests confirmed residual strengths above 100%, indicating excellent long-term stability. Microstructural analyses confirmed ettringite formation in CBA and both ettringite and C–S–H gel in IBA, explaining the superior performance of IBA. Overall, the findings establish ALCCOFINE-stabilized CBA and IBA as low-carbon, resource-efficient materials suitable for embankments, subgrades, and sub-

	base layers in both rural and national highway projects, contributing to sustainable infrastructure development.
78.	Supramolecular nano-assembly of melatonin-conjugated peptide as a multifunctional scaffold for wound healing applications **P Bundel, P Shounak, A Vashisth, Y Singh** - Biomacromolecules, 2026 **Abstract:** Wounds are one of the major socioeconomic challenges globally, mainly arising from trauma, surgery, burns, and infections. In many cases, prolonged recovery time leads to complications and requires a multifunctional approach that can target tissue regeneration and prevents infection. The supramolecular assembly of peptides yield well-defined nanoassemblies that resemble the extracellular matrix and influence cellular interactions. The peptide-based systems allow structural fine-tuning, high biocompatibility, and the ability to incorporate bioactive signals. Despite advances in peptide-based supramolecular gels for wound treatment, multifunctional peptide-based scaffolds remain relatively unexplored. In this work, we have designed a melatonin-conjugated amphiphilic peptide that self-assembles into a viscoelastic, nanofibrous gel with antibacterial and wound-healing functions. The amphiphilic nanofibers effectively disrupted bacterial membranes, and conjugated melatonin enhanced the antioxidant activity and promoted M1 to M2 macrophage polarization. The structural and biological properties of the self-assembled gel provide a promising multifunctional platform for wound management.
79.	Targeted β-glucan-veiled oral apremilast nanotherapy modulates key dysbiosis-associated gut microbiota and alleviates ulcerative colitis-associated anxiety, depression, and neuropsychiatric behaviors C Jori, A Shaney Rehman, **T Lamba…JN Agrewala, R Khan** - Advanced Science, 2026 **Abstract:** Oral nanomedicines that modulate gut microbiota and gut–brain interactions are crucial for effectively treating inflammatory bowel disease (IBD) and associated psychiatric disorders, such as anxiety and depression. However, the underlying causes of psychiatric disorders in patients with IBD remain unclear, and effective treatment strategies have yet to be established. Herein, we developed oral gastroprotective βG@Apr-WPG NMs (β-glucan armored apremilast encapsulating tryptophan-poly(lactic-co-glycolic acid)-glutathione nanomicelles). This system effectively treats IBD and associated anxiety/depression by modulating the microbiota–gut–brain axis. βG@Apr-WPG NMs demonstrated gastroprotection enhances retention, and enables sustained release within the inflamed colon, enhances drug solubility, and inflammation-responsive apremilast release significantly improving oral therapeutic efficacy. Oral βG@Apr-WPG NMs administration outperformed free apremilast by restoring gut barrier integrity, reducing histopathological damage, and modulating microbial dysbiosis. Systemic inflammation and neuroinflammation were markedly suppressed. Notably, the βG@Apr-WPG NMs ameliorated anxiety- and depression-like symptoms, as well as cognitive deficits in colitis-induced mice, highlighting its therapeutic impact beyond the gut. Addressing reduced efficacy of conventional therapies, this multifunctional βG@Apr-WPG NMs platform offers safe, simple, and highly efficient therapeutic strategy integrating targets intestinal inflammation, microbiota–gut–brain axis modulation, in the pathogenesis of IBD with comorbid neuropsychiatric disorders with confirmed safety.
80.	"The goddess is singing on a neem branch" nature-anthropic harmony in magahi song-texts RK Pankaj, **D Ray** - Environmental Humanities, 2026 **Abstract:** At the overlap of Indigenous and religious tradition, ethnomusicology and ecocriticism, this article offers a detailed thematic analysis of Magahi folk songs, an Indigenous oral tradition of Hinduism practiced in the Magadh region of eastern India. Focusing on the theme of harmony between nature and human beings, this article argues that Magahi folk culture provides a unique perspective in modern ecocritical thoughts by answering the recurrent questions asked by the

	discipline. Ecocriticism, throughout its three-decade history, has repeatedly queried whether nature can be perceived in nonanthropocentric terms by removing the human being as the sole purveyor and savior of ecology. This article argues that—in spite of the vast geopolitical difference between Western ecocriticism and Indian ethnic culturalism—the Magahi song-texts can be read as a nonanthropocentric philosophy that regards nature as an irreducible, agential deity that should be feared/revered, avoided/pleaded to, collaborated with/worshipped by the human beings. Divided into two parts, this article first discusses the discourse of perceiving nature while avoiding anthropocentrism, then posits the archived and translated samples of Magahi song-texts as a possible response, providing an intersection of academic theory and pragmatic, Indigenous eco-activism
81.	Thermal and microstructural analysis of laser remelting of cold-sprayed copper coating **J Kumar, P Kumar, DK Goyal, R Kant, H Singh** - CIRP Journal of Manufacturing Science and Technology, 2026 **Abstract:** Sometimes cold-sprayed coatings may exhibit a challenge of porosity, weak intersplat bonding, and uneven surface due to the solid-state deposition process. Laser remelting has the possibility to eliminate these defects by promoting localized melting, material flow, and microstructural refinement. This study investigates the temperature field and microstructural evolution during laser remelting of cold-sprayed copper coatings deposited on a low-melting-point Al 6061 substrate. Copper coatings were deposited using the cold spray (CS), followed by the development of a finite element-based heat transfer model to analyze the temperature distribution and to identify optimal laser parameters that enable remelting of the coating without damaging the interface of the substrate. The numerical model was validated experimentally by comparing the predicted surface temperatures with measurements obtained from a thermal imaging camera, showing good results with an error of only 7–9%. The temperature analysis shows that a 1000 W laser power and 100 mm/min scan speed during the second pass provide optimal conditions for proper remelting of the Cu coating, while preserving the Cu-Al interface. Compared with the as-sprayed condition, laser remelting significantly improved the coating quality by reducing porosity and surface roughness. The reduction in microhardness after remelting was attributed to stress relaxation and thermal softening associated with the reduction of the work-hardening effect. Quantitatively, the porosity decreased from 7.2% to 3.2%, and the surface roughness decreased from 10.5 µm to 5.0 µm, while the microhardness decreased from 103 $HV_{0.3}$ to 63 $HV_{0.3}$ as the scan speed varied from 150 to 50 mm/min. These results show that laser remelting is an effective post-treatment technique for enhancing the coating properties and quality of cold-sprayed copper coatings for advanced engineering applications.
82.	Thiolated chitosan-stearic acid thiol-linked biomimetic hydrogels for axonal regrowth and neuronal tissue regeneration **M Bhatt, B Das** - ACS Applied Bio Materials, 2026 **Abstract:** Neuronal disorders like spinal cord injury, stroke, peripheral neuropathy, and neurodegenerative diseases like Alzheimer's disease, Parkinson’s disease, etc., need regenerative approaches and therapeutics like tissue engineering and cell therapy for neuronal systems. Significant factors such as neuronal damage, impaired immune response, and glial scar formation create a hostile environment for neural repair and functional recovery. To overcome these challenges, the development of biocompatible and bioactive biomaterials is essential for therapeutic applications. In this work, a thiolated chitosan-stearic acid (Tch-Sa) hydrogel was prepared by modifying chitosan and stearic acid with free thiol (SH) groups, mimicking the high lipid content and GaGs in neuronal tissue. The hydrogel was crosslinked via disulfide linkages. The hydrogels were characterized using FTIR, ^{1}H NMR, Raman spectroscopy, and TGA. Rheological evaluation demonstrated stable mechanical behavior, with storage and loss moduli

	showing structural consistency. In vitro cytocompatibility studies with N2a neuronal cells showed good adhesion, proliferation, and gradual morphological development. By day 7, cells displayed extended axonal projections. Immunofluorescence staining revealed increased expression of neuronal proteins, supporting the hydrogel's role in promoting neuronal differentiation and maturation. Moreover, the introduction of thiol groups enhanced cell permeability, mucoadhesive properties, and axonal outgrowth, suggesting that this material may be helpful in neuronal tissue engineering applications. 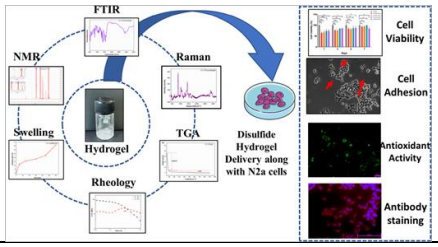
83.	Topology-aware task mapping strategies for S-NUCA based many-core architectures A Jain, **J Singh,** AS Anand, V Subramanian - Software: Practice and Experience, 2026 **Abstract:** Background Task scheduling in many-core systems with static non-uniform cache access (S-NUCA) is complicated by spatial variability in cache latency and thermal hotspots. Prior research has considered cache asymmetry, inter-thread distance, and locality, but these factors are often treated separately and predominantly within runtime-based frameworks rather than being integrated into a unified compile-time strategy. Objective To develop compile-time topology-aware thread mapping strategies that jointly address spatial cache locality and thermal constraints without incurring runtime migration overhead. Methods We propose three compile-time thread mapping strategies, namely Golden-Angle Spiral Mapping (GASM), Max Distance Anti-Cluster Mapping (MDAC), and Latency-Aware Minimal Mapping (LAMM). These approaches leverage geometric dispersion and Average Manhattan Distance (AMD) between cores to enhance spatial placement. Each mapping targets a distinct scenario, with LAMM designed for low-thread compute-bound workloads, MDAC for high-thread thermally constrained cases, and GASM for irregular memory-intensive workloads. These methods statically address thermal and latency constraints without runtime migration overhead, enabling low-complexity mappings with predictable performance and thermal behavior. Results Across 8, 12, 16, and 64 thread configurations, the proposed topology-aware mappings achieve up to 26% performance improvement and 16% energy reduction over the static baseline. Even when compared with the dynamic baseline, which benefits from runtime adaptation, they continue to deliver up to 20% higher performance and 9% lower energy consumption. Under workload-specific thread configurations, performance gains reach 22% and energy savings 18%, with each mapping showing the benefit for its target workload behavior. Overall, these results validate the effectiveness of a complementary multi-strategy approach for thermally constrained S-NUCA many-core systems.
84.	ZrO2 crystal phase mediated surface synergistic effect of Ni-ZrO2 for tuning furfural hydrogenation and rearrangement pathway in aqueous medium **V Garule, AK Manal, T Mondal, R Srivastava** - Applied Catalysis B: Environment and Energy, 2026 **Abstract:** Efficient and selective regulation of reaction pathways for furfural (FFR) hydrogenation to achieve desired products under identical conditions is enormously strenuous. Design and understanding of active sites for FFR adsorption, activation, and reaction-pathway tuning are pivotal to addressing this challenge. In this work, two distinct crystal structures of ZrO 2 -supported Ni catalysts are developed for the hydrogenation of FFR to tetrahydrofurfuryl alcohol (THFA) and rearrangement to cyclopentanone (CPO) under mild conditions in water. Ni/t-ZrO 2

	(t = tetragonal) preferentially promotes furan-ring hydrogenation to THFA with 92.5% yield, whereas Ni/m-ZrO 2 (m = monoclinic) selectively affords 91.4% rearranged product (CPO = 83.4% and cyclopentanol (CPL) = 8%), under identical reaction conditions (130 °C, 2.0 MPa H 2 , 5 mL water). The catalyst characterization, kinetic studies, control experiments, and FTIR adsorption reveal that electron-rich, highly dispersed Ni sites over Ni/t-ZrO 2 promote planar FFR adsorption, enabling rapid FFR hydrogenation and subsequent spillover-assisted ring hydrogenation to THFA. In contrast, Ni/m-ZrO 2 exhibits slower initial hydrogenation but strong acid sites rapidly convert the intermediate via acid-assisted ring-opening and rearrangement to CPO through a consecutive, substrate-assisted mechanism. The distinct catalytic functionalities of Ni–ZrO 2 highlight phase-dependent selectivity across diverse biomass-derived feedstocks, demonstrating precise crystal-phase–driven synergy between hydrogenation and C–O bond cleavage pathways.